LS Scienza dei Materiali - a.a. 2008/09

Fisica delle Nanotecnologie – part 4

Version 7 Oct 2008

Francesco Fuso, tel 0502214305, 0502214293 - fuso@df.unipi.it
http://www.df.unipi.it/~fuso/dida

Tecnologie non-ottiche ed emergenti per la nanofabbricazione

Outlook

1. Further reducing the wavelength: the use of charged beams
2. Basics of electron microscopy: TEM, SEM
3. Electron beam lithography: advantages and technological limitations
4. Other charged-beam techniques: SCALPEL and FIB
5. An approach based on atom optics: atomic nanofabrication
6. A few emergent techniques:
   i. Nanoimprint;
   ii. Multiphoton and direct writing of 3D (nano)structures;
   iii. The inkjet printer (!)

1. Use of charged particle beams

Da Brandon Kaplan
Microstruct. Charact.
of Materials
Wiley (1999)

Matter waves instead of radiation

Basic components:
- electron optics;
- accelerated particles

First "peculiarities" of the implementation:

- Large kinetic energy (tens of KeV) → possible sample damages

- Care required to fix the electric potential → typ. applied to conductive substrates

- Need for UHV environment

- Inherently **serial (scanning) technique**

4.1.1 Wave Properties of Electrons

The focusing of an electron beam is possible because of the dual, *wave–particle* character of electrons. This wave–particle duality is expressed in the *de Broglie relationship* for the wavelength of a particle:

$$\lambda = h/mv \tag{4.1}$$

where m is the mass of the particle, v is its velocity and h is the Planck constant. Assuming that the accelerating voltage in the electron gun is V, then the electron energy is given by:

$$mv^2/2 = eV \tag{4.2}$$

where e is the charge on the electron. It follows that $\lambda = h/(2meV)^{0.5}$, or $\lambda = (1.5/V)^{0.5}$ nm when V is in volts. This numerical value is approximate, since at the accelerating voltages commonly used in the electron microscope, the *rest mass* of the electron, m_0, is appreciably less than the *relativistic mass*, m, and a correction term should be included, in the equation:

$$\lambda = \frac{h}{\sqrt{\left[2m_0eV\left(1+\frac{eV}{2m_0c^2}\right)\right]}} \tag{4.3}$$

where c is the velocity of light. The relativistic correction amounts to *ca* 5 % at 100 kV, rising to 30 % at 1 MV. The electron wavelength at 100 kV is 0.00370 nm, which is nearly two orders of magnitude less than the interatomic spacings typical of the solid state. At 10 keV, which is typical of many applications of scanning electron microscopy, the wavelength is only 0.012 nm, still appreciably less than the interatomic distances in solids.

de Broglie wavelength is much smaller than radiation wavelength → diffraction has negligible effects

Electron microscopy I

As in optical methods, microscopy (**TEM, SEM**) and lithography (**EBL**) are two faces of the same topic also in electron-based methods

Before discussing electron lithography, **electron microscopy** must be introduced

As in optical microscopy, both “reflection” and “transmission” of the electron beam from the sample can be acquired, leading to **SEM** and **TEM**, respectively

An electron passing through a solid may be scattered
* not at all
* once (single scattering)
* several times (plural scattering), or
* very many times (multiple scattering)

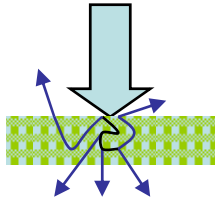

Each scattering event might be elastic or inelastic. The scattered electron is most likely to be forward scattered but there is a small chance that it will be backscattered.

The probability of scattering is described in terms of either an "interaction cross-section" or a mean free path. When the solid specimen is thicker than about twice the mean free path, plural scattering is likely.

The important features are the fraction of electron scattering forward and backwards and the volume of the specimen in which most of the interactions (scattering events) take place.

http://www.matter.org.uk/tem

Electron microscopy II

There are four main processes by which a high energy electron (red here) can lose energy to an atom.
These are

1. The excitation of a plasmon
2. The excitation of a single electron from the valence band (pale green)
3. The excitation of an inner shell electron (from the K or L shell)
4. The excitation of a phonon

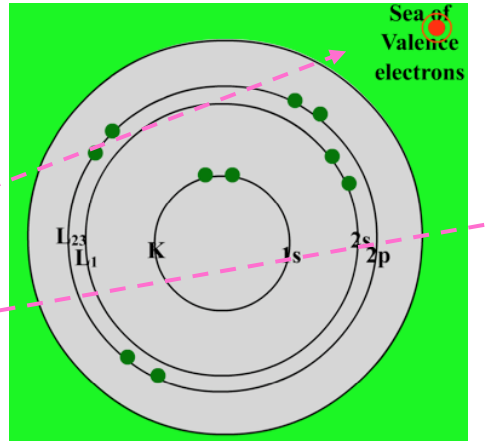

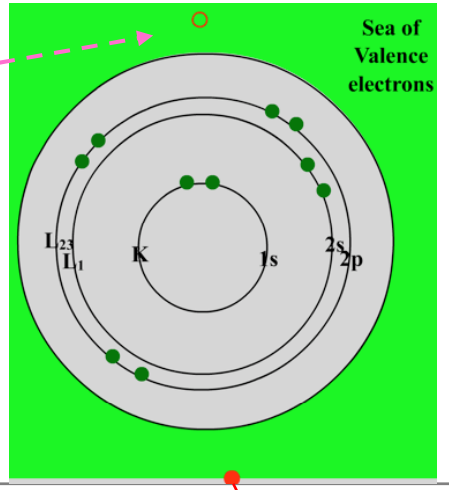

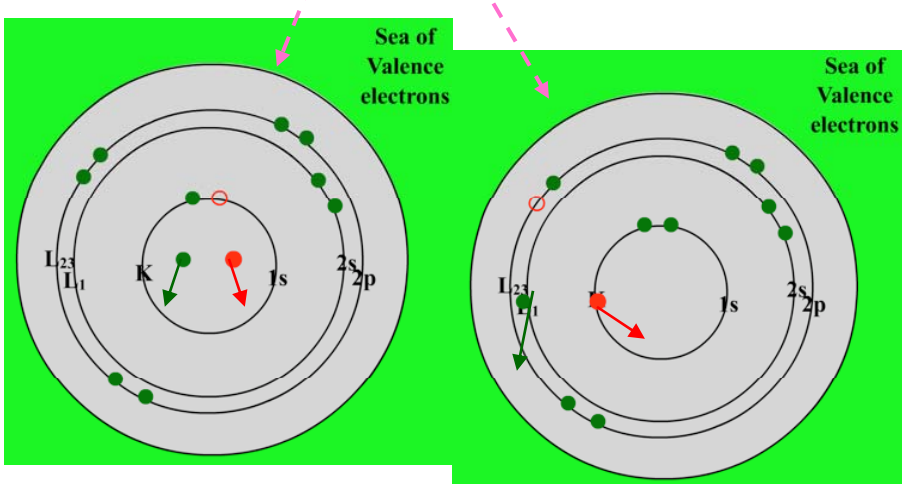

After an inner shell excitation an atom has an energy above its ground state. It can relax and lose some of this energy in several ways, of which two are described here. Both start with an outer electron jumping in to fill the vacancy in the inner shell.

Characteristic X-ray emission. Energy is given off as a single X-ray photon.

Auger electron emission. Energy is given off by one of the outer electrons leaving. It carries a characteristic kinetic energy.

http://www.matter.org.uk/tem

Reminders on Auger effect

Quando un atomo viene colpito da un elettrone di energia sufficientemente elevata può avvenire che un elettrone degli strati più interni (elettrone di core) venga espulso originando una vacanza elettronica. La configurazione risultante corrisponde ad un sistema atomico di tipo metastabile e accade che un elettrone appartenente ad un livello energetico più esterno va ad occupare la vacanza creatasi, processo a cui corrisponde un conseguente rilascio di energia. Questa energia può essere emessa in forma radiativa sotto forma di onda elettromagnetica: si avrà emissione di raggi X, in quanto il fotone prodotto appartiene a tale parte dello spettro. Non sempre però l'energia rilasciata viene convertita nella produzione di un fotone in quanto può anche accadere che questa energia venga ceduta ad un terzo elettrone, del guscio più esterno, che riesce così a raggiungere il livello di vuoto e a fuoriuscire dalla materia. Questo processo rappresenta l'emissione Auger e l'elettrone espulso in seguito a tale fenomeno è detto **elettrone Auger**.

L'energia cinetica dell'elettrone Auger espulso dipende esclusivamente dall'energia dei 3 livelli energetici coinvolti nel processo:

$$E_{cin} = E_1 - E_2 - E_3 - E_{WF}$$

dove

E_1 è l'energia del livello atomico su cui vi è la vacanza che determina lo stato metastabile dell'atomo.

E_2 è l'energia del livello energetico che occupava il secondo elettrone prima di andare a riempire il posto liberatosi.

E_3 è l'energia del livello energetico del terzo elettrone che verrà emesso per effetto Auger.

E_{WF} è la *working function*, cioè una funzione che rende conto del lavoro necessario per poter espellere l'elettrone Auger.

L'effetto Auger è alla base della spettroscopia Auger (AES), una delle maggiori tecniche di analisi di superficie.

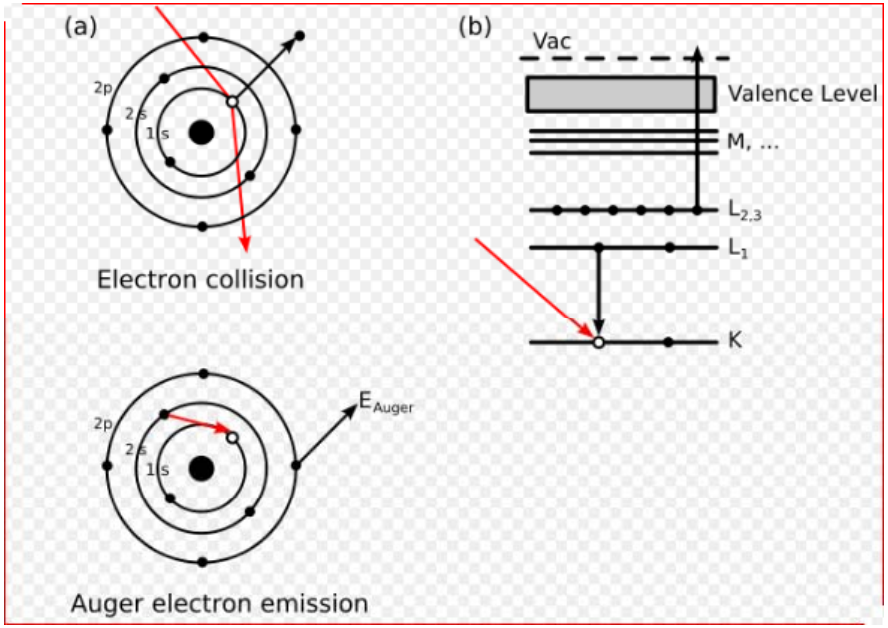

Figure 1. Two views of the Auger process. (a) illustrates sequentially the steps involved in Auger deexcitation. An incident electron creates a core hole in the 1s level. An electron from the 2s level fills in the 1s hole and the transition energy is imparted to a 2p electron which is emitted. The final atomic state thus has two holes, one in the 2s orbital and the other in the 2p orbital. (b) illustrates the same process using spectroscopic notation, $KL_1L_{2,3}$.

2. Components of TEM, SEM, EBL

Bright electron sources

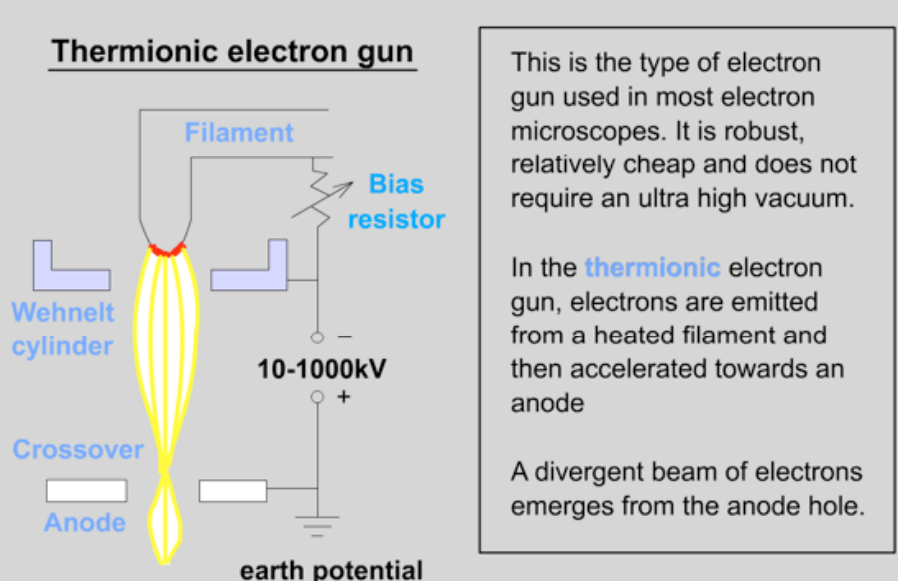

Electron optics (lenses, condensers, etc.)

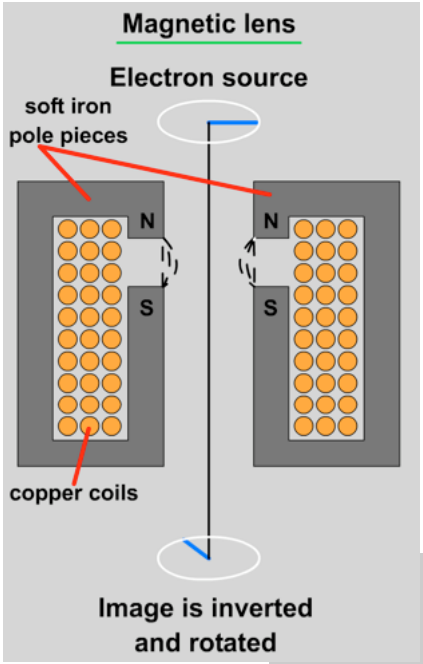

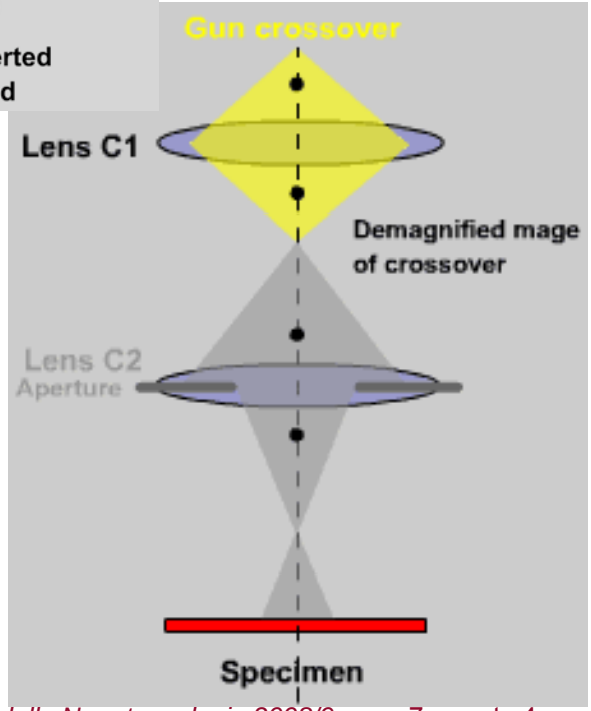

In the TEM, higher energy electrons permit the examination of thicker specimens, but may cause specimen damage. Higher voltage microscopes are also more expensive. Most TEMs have a maximum HT of ~ 200kV. In the SEM, the maximum HT is usually ~ 25kV and its choice is determined by a compromise between penetration (which increases with HT) and beam diameter (which decreases with HT).

Penetration strongly depending on material and electron energy (typ range 1-100 nm)

Field emission

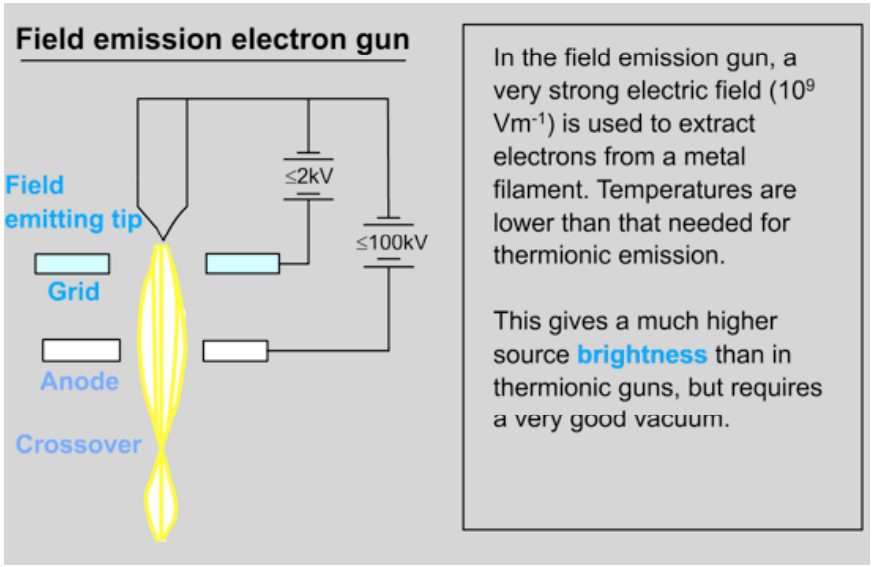

This carbide crystalline tip, with a radius of 100 angstroms, or 10 nanometers at the top and 0.5 micron at the base, emits electrons in a tiny beam.

Field and thermionic emission and photoemission

(From Lindquist et al., *Research and Development*, June, 91–98, 1990. With permission.)

Electron emission in a water bucket

THE THREE MECHANISMS used by field emission sources all basically involve emitting electrons and ions from a metal surface under the influence of a strong electric field.

Understanding these mechanisms is where the water bucket comes in.

In this analogy, the water level in a bucket represents the Fermi level—the highest occupied energy level in a cathode material. The work function is the energy required to get the water droplets (electrons) from the top of the liquid out of the bucket. This is the distance equivalent to the potential energy barrier.

In photoemission, photon energy excites electrons at the Fermi level of the cathode material and can impart enough kinetic energy to allow the electrons to escape from the bucket.

In thermionic emission, heat thermally excites the electrons, providing enough energy to boil the electrons off and out of the bucket.

In field emission a high electric field can thin the side of the bucket enough so that the electrons can tunnel through it.

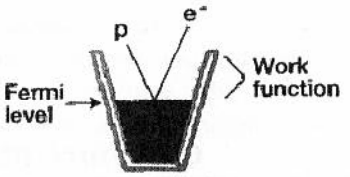

Photoemission

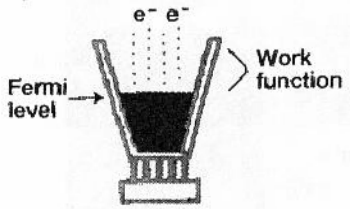

Thermionic emission

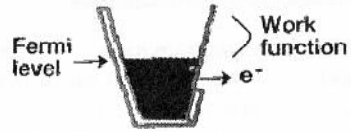

Field emission

"Tip effect" can enhance field emission
→ micro/nanofabricated field emitters (also nanotubes??)

Contrast mechanisms I

Basically:

- in **TEM** electrons "transmitted" by the sample are analyzed;
- in **SEM** electrons "scattered out" ("reflected") from the sample are analyzed

In case of TEM, sample must be thinned in order to be "semi-transparent"

Figure 16: Schematic procedure to prepare a planar sample for TEM. After preparing the sample on an substrate the latter may be etched. The final thickness of some 100 nm can be achieved by ion milling. The up pointing arrows denote the direction of the TEM beam.

(…a complicated and destructive procedure!!)

Mostly, cross-sections are imaged with TEM

Since the electron wavelength is close to typical lattice spacing (or any other length of interest for a solid medium), Bragg diffraction by the sample microstructure do play a role

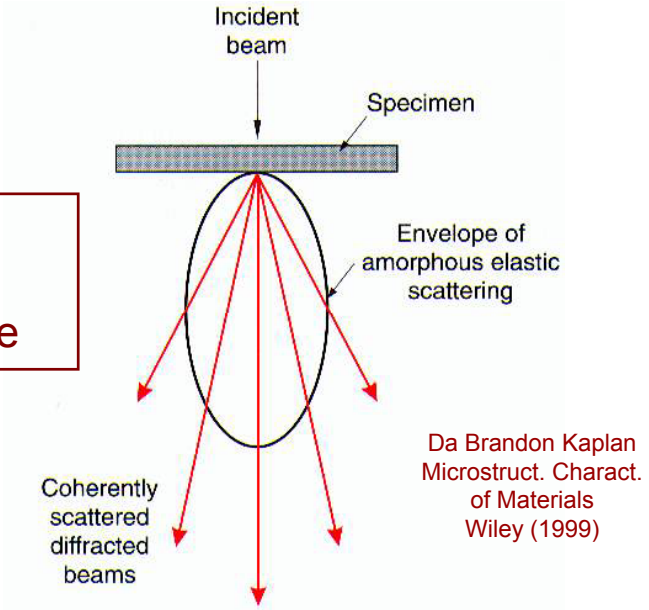

Da Brandon Kaplan
Microstruct. Charact.
of Materials
Wiley (1999)

Contrast mechanisms II

In TEM, where elastic interaction is predominant; main contrast mechansims are:

1. **mass thickness** (transmission depends on the amount of mass crossed by the electrons)
2. **diffraction** (in crystalline materials Bragg diffraction plays a role leading to high sensitivity to lattice defects)
3. **phase contrast** (when collection optics has a large numerical aperture, due to mutual interference of many diffracted beams)

Morphological, structural, and topographical information are somehow "convoluted", but space resolution can be excellent

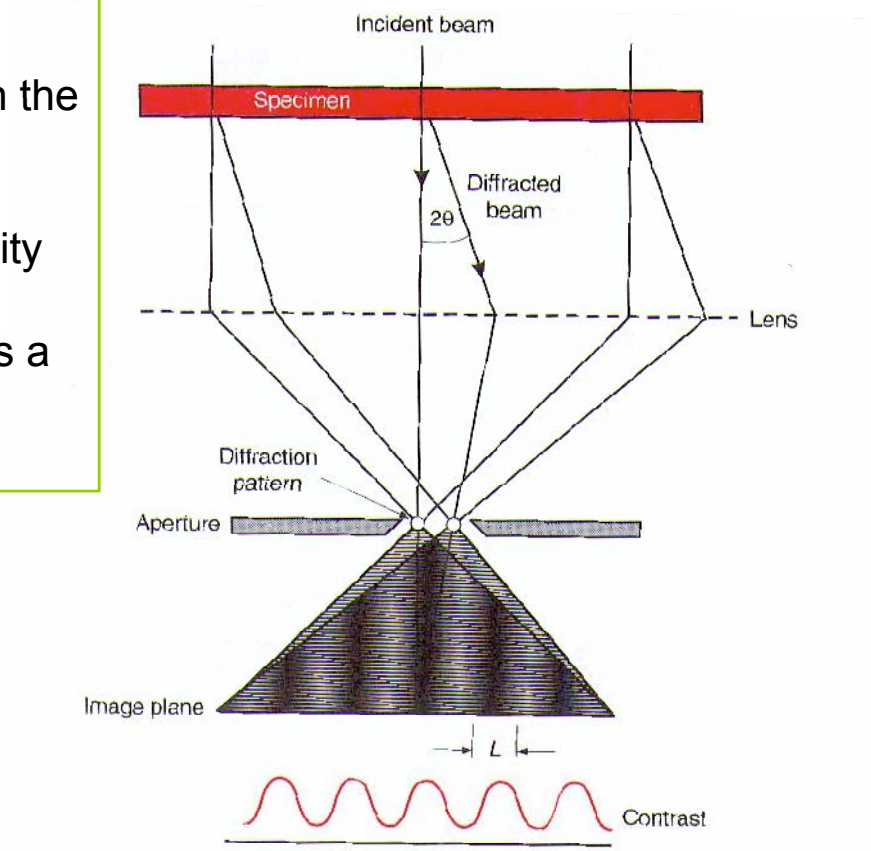

Figure 4.15 If the objective aperture accepts a Bragg-diffracted beam as well as the direct transmitted beam, $\alpha > 2\theta$, then an interference pattern will be formed in the image plane as a result of the difference in path lengths of the two beams

Bright and dark field images

By inserting the aperture or tilting the beam, different types of images can be formed.
The most common conditions are:

* No aperture - the diffraction pattern is centered on the optical axis.
* Aperture is centred on the optical axis.
* Aperture displaced, selecting a diffracted beam.
* Beam is tilted so that the diffracted beam is on the optical axis.

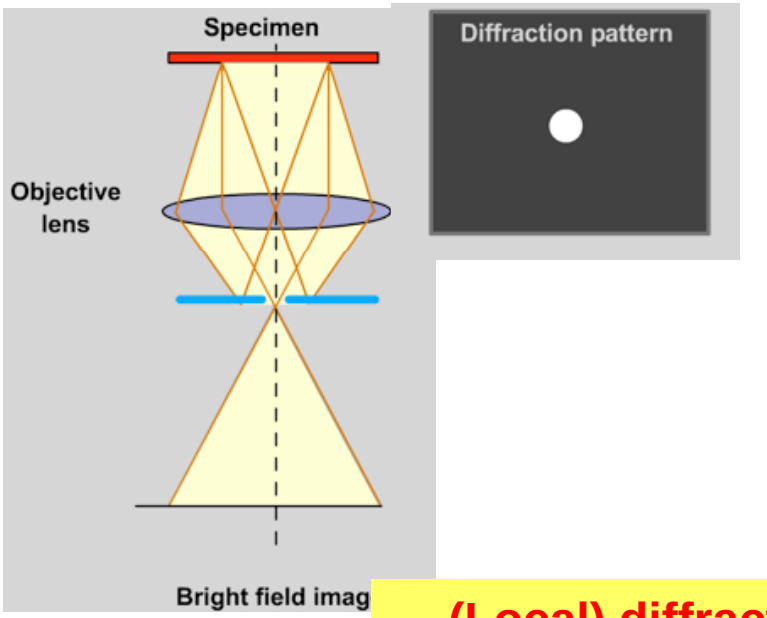

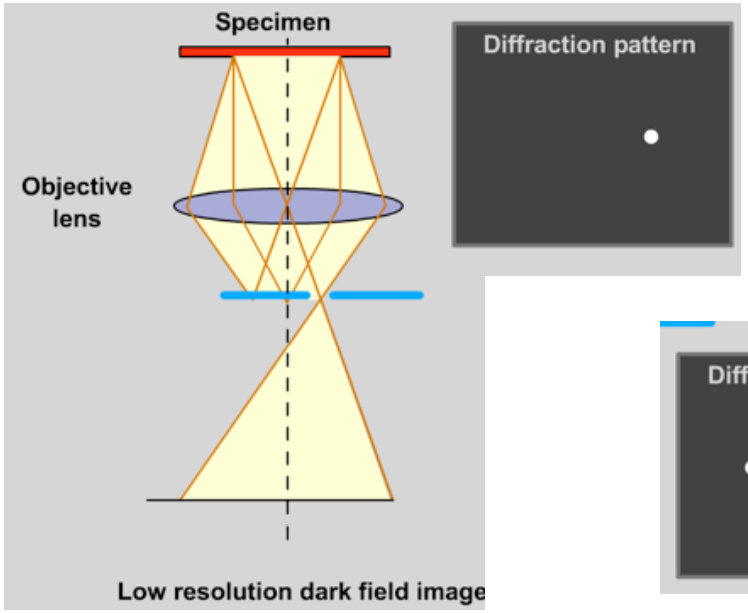

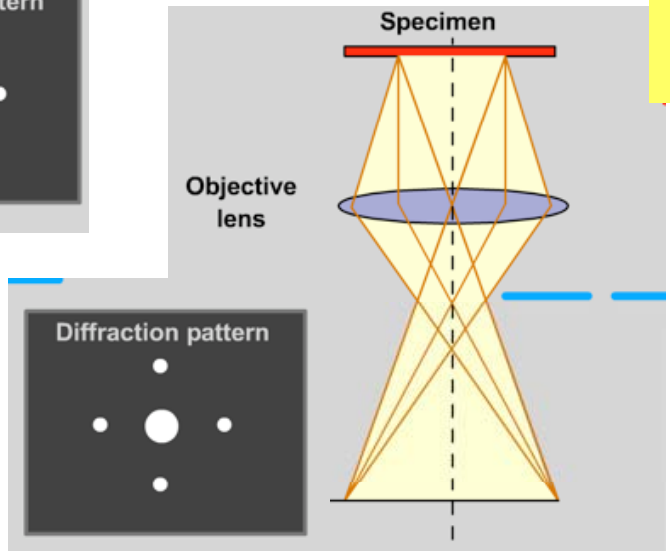

(Local) diffraction patterns can be acquired with TEM

Scanning TEM

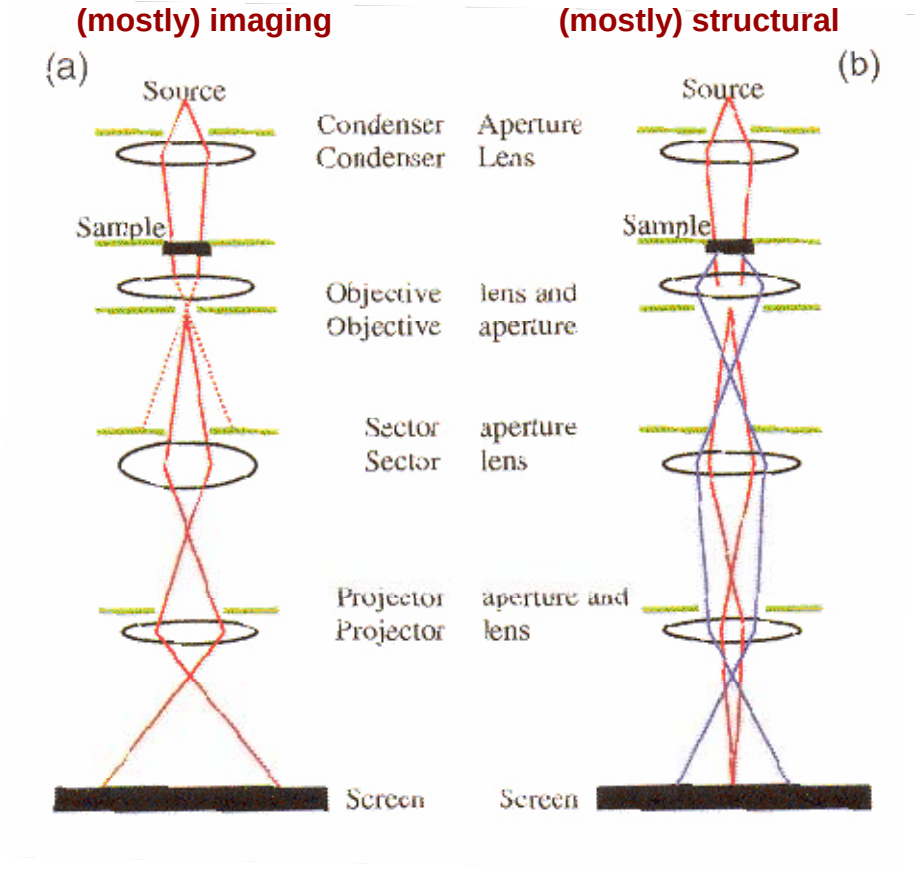

Need for UHV
Inherently serial technique
Sample preparation needed (including potential control, e.g., metallization, grounding)

Frequently, the electron beam is scanned across the sample surface
(*a relatively slow process!!*)

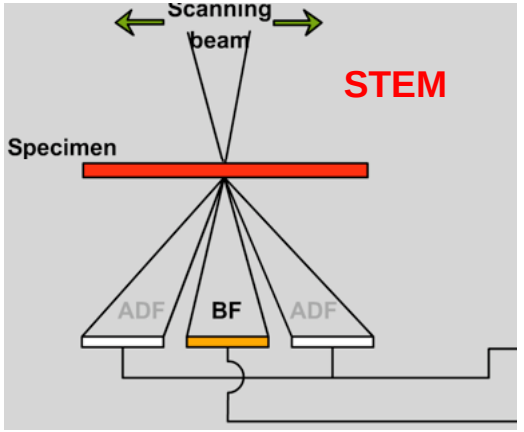

STEM image formation:

A Bright Field (BF) detector is placed in a conjugate plane to the back focal plane to intercept the direct beam while a concentric Annular Dark Field (ADF) detector intercepts the diffracted electrons.

Examples of high resolution TEM I

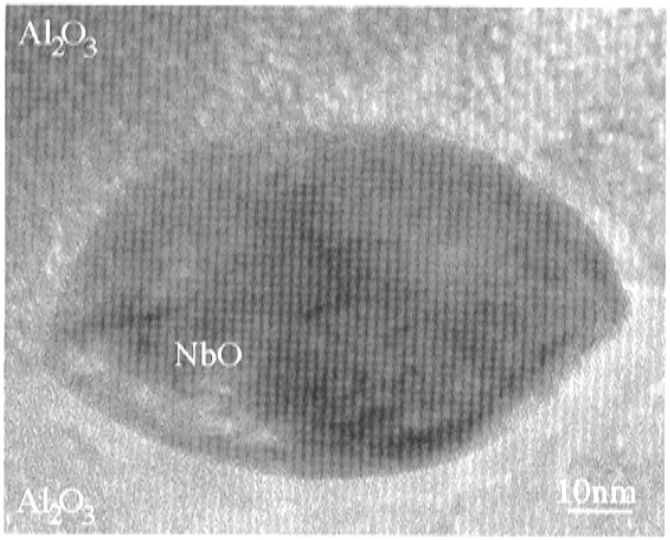

Figure 4.53 Transmission electron micrograph of a NbO particle located at a grain boundary in polycrystalline alumina. Phase contrast (lattice fringes) and mass–thickness contrast vary from the alumina grain to the NbO grain

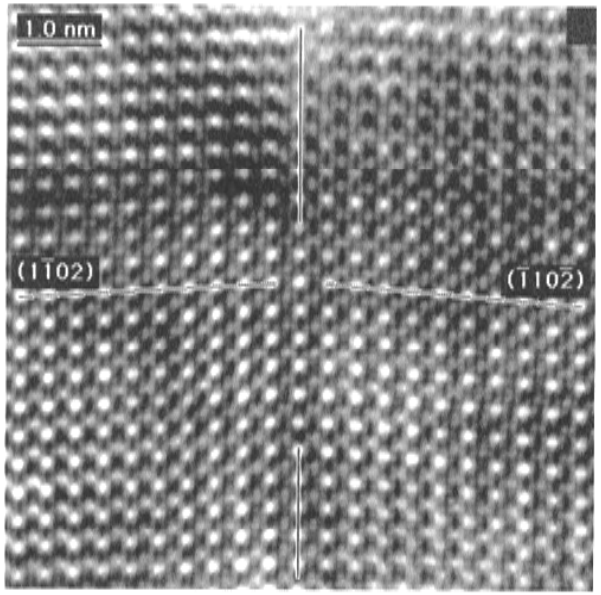

Figure 4.54 Lattice image of a rhombohedral twin in alumina

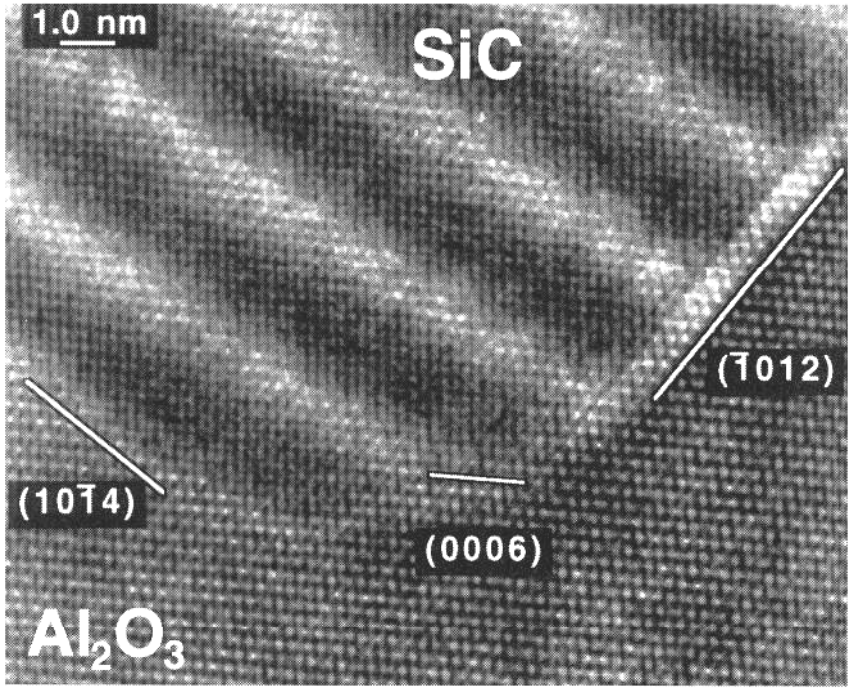

Figure 4.55 Lattice image of a SiC particle located within an alumina grain. The alumina lies along a low-index-zone axis, and is the source of the lattice image. A moiré pattern appears within the SiC particle due to overlap between the alumina and SiC (in the direction of the electron beam)

Atomic resolution achieved along with structural information
(in crystalline samples!)

Examples of high resolution TEM II

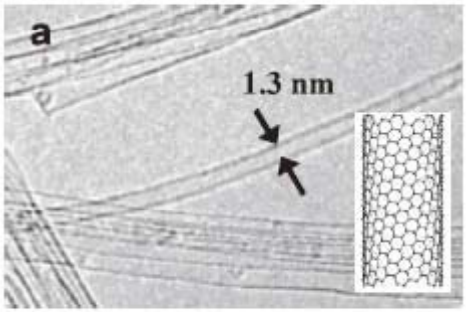

CNH is a nanometric carbon tubes taking a horn or cone shapes at the tip. This material has five five-membered rings on the extremity of the horn. As shown in the transmission electron microscopy images shown in Fig. 1(b) and (c), some thousands of horn structures are usually assembled into a spherical shape by orienting their extremities toward the outside and this shape somewhat resembles a chestnut bur or a sea urchin. This assembly has a diameter of from 80 to 100 nanometers. The CNH structure is distorted due to the presence of some five- or seven-membered rings, but the assembly is stable because these structures are bonded at the center.

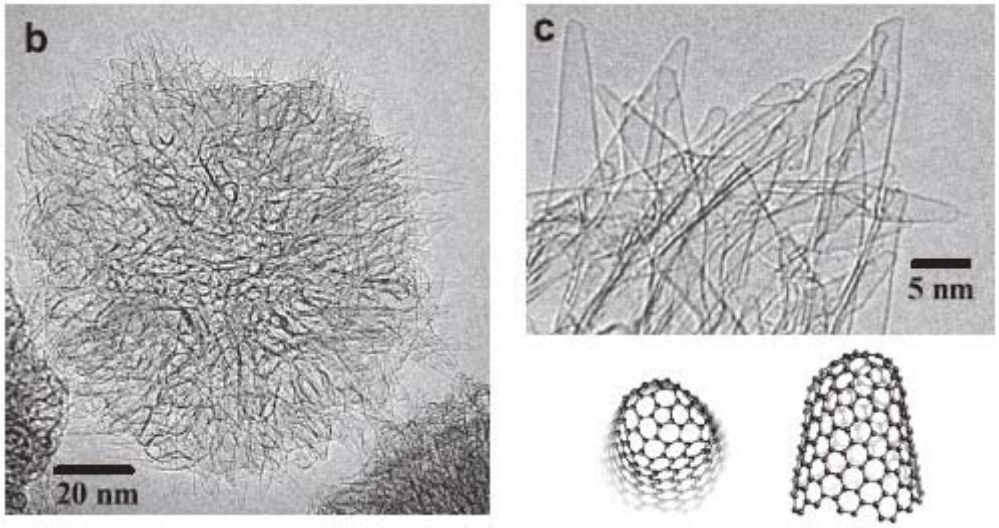

Fig. 1 Transmission electron microscopy images of CNT (a) and CNH (b), (c). Inserted illustrations are CG images of CNT and CNH respectively.

Isolated nanostructures (supported by suitable substrates, hence duly prepared) can be imaged as well by TEM (or STEM)

Examples of high resolution TEM III

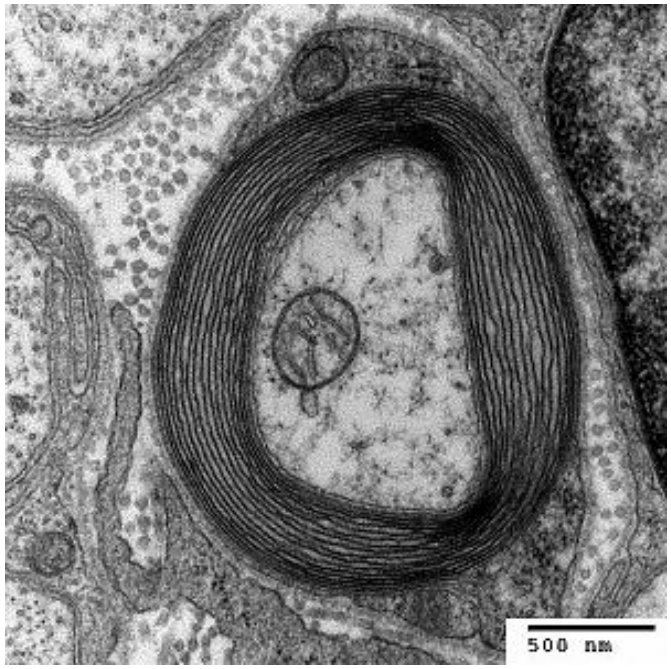

Transmission electron micrograph of a myelinated axon. Generated at the Electron Microscopy Facility at Trinity College, Hartford, CT

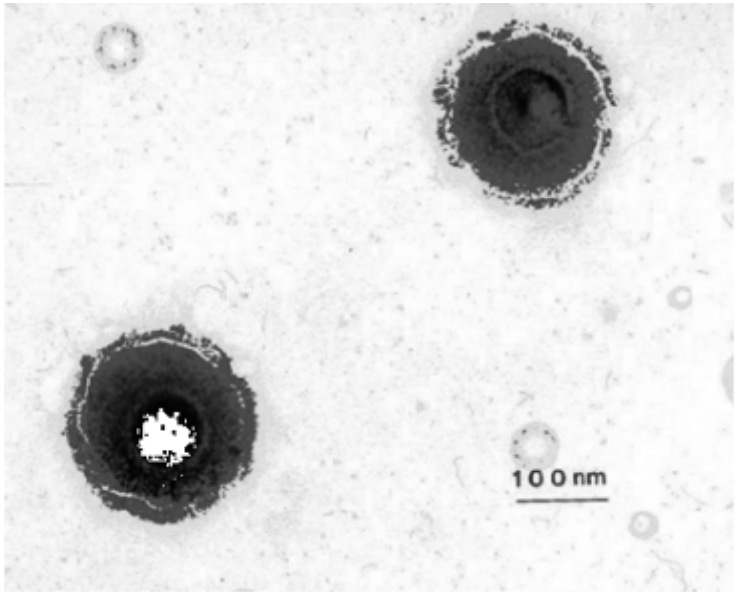

Two herpes virus particles are shown; they were prepared for transmission electron microscopy by the negative stain technique.

Different materials (including biologics) can be imaged, after suitable preparation (e.g., cross sections, metallization, staining, etc.)

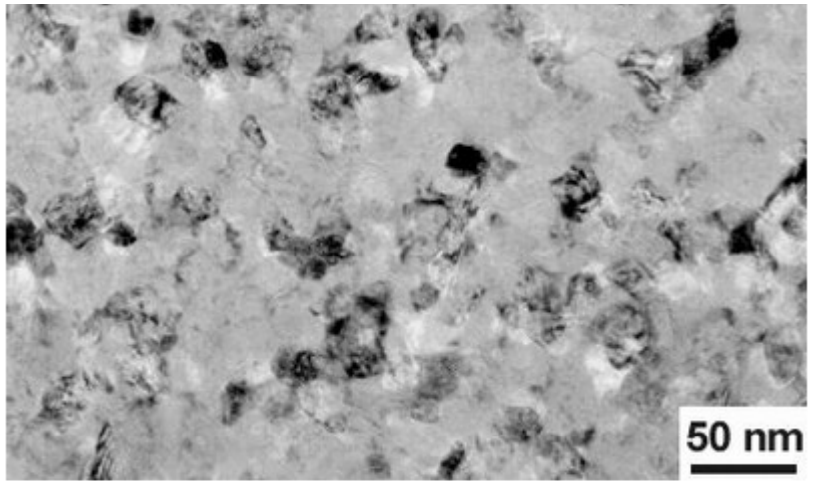

TEM brightfield image of Ni grains in thin film

Comments on space resolution

A new microscope developed by the TEAM Project (Transmission Electron Aberration-corrected Microscope), supported by the U.S. Department of Energy, has recorded the highest-resolution images ever seen (0.05 nanometer and below). This is equivalent to a quarter of the diameter of a carbon atom. This microscope will be delivered to the Berkeley National Laboratory in 2008 and will be fully operational in 2010. To achieve this resolution, this microscope mixes two technologies, SEM (Scanning Electron Microscope) and TEM (Transmission Electron Microscope). Such a microscope will allow to 'study how atoms combine to form materials, how materials grow and how they respond to a variety of external factors.'

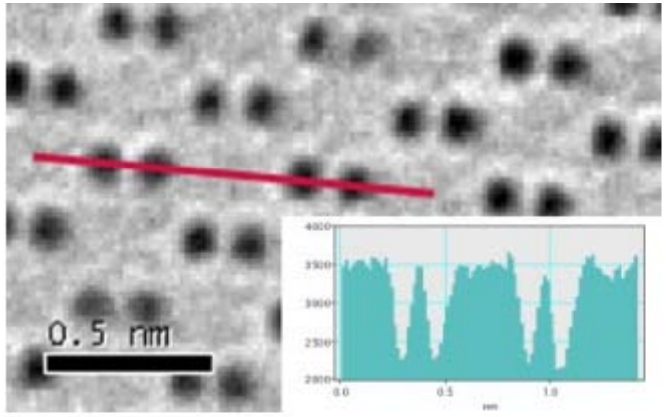

You can see above "a high resolution TEM image of the dumbbell structure (0.14nm) of Germanium, which reveals that inter atomic distances can be measured with ultrahigh precision. The intensity profile (insert) brilliantly proves that the contrast level in between the germanium dumbbell reaches the base level of the larger distances of the structure." (Credit: FEI Company)

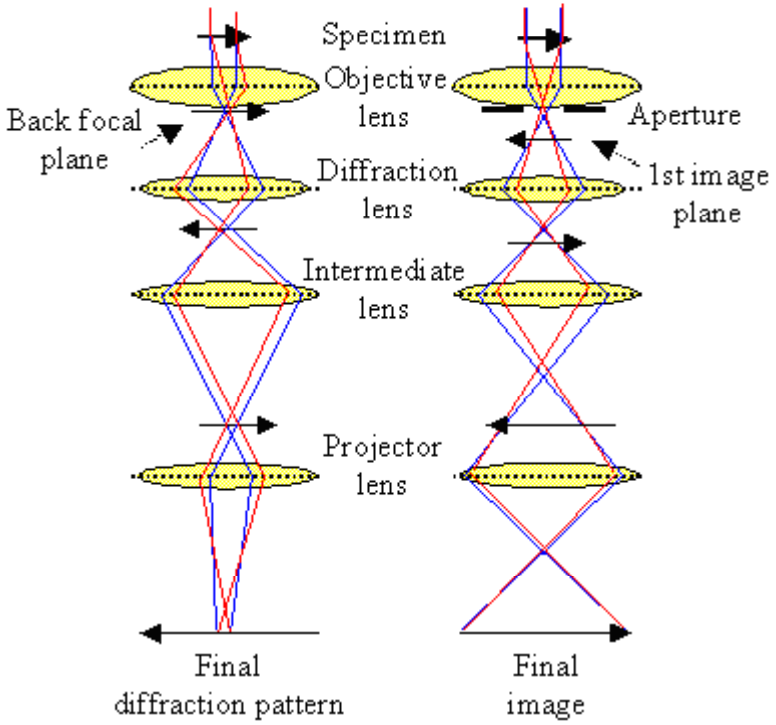

In TEM, spatial resolution is not directly related to the probe (the e-beam) size, but depends on the highly local character of the contrast mechanisms

The transmitted e-beam, space-modulated due to mass thickness, diffraction, phase contrast, etc., is imaged having been magnified at a level compatible, for instance, with intensified CCD resolution (1 pixel ~ 5-20 μm)

Scanning electron microscopy

There are two types of electron microscopes: the transmission (TEM) and the scanning tunneling (STM) electron microscope. In a TEM, a monochromatic beam of electrons is accelerated through a potential of 40 to 100 kilovolts (kV) and passed through a strong magnetic field that acts as a lens. The resolution of a modern TEM is about 0.2 nm. This is the typical separation between two atoms in a solid. This resolution is 1,000 times greater than a light microscope and about 500,000 times greater than that of a human eye. The STM is similar to the TEM except for the fact that it causes an electron beam to scan rapidly over the surface of the sample and yields an image of the topography of the surface. The resolution of a STM is about 10 nm. The resolution is limited by the width of the exciting electron beam and by the interaction volume of electrons in a solid.

Typ. Filament source (ddp 10-100 kV):
W: j~5x10^4 A/m^2
LaB_6: j~1x10^6 A/m^2
field emitter: j~5x10^{10} A/m^2!!

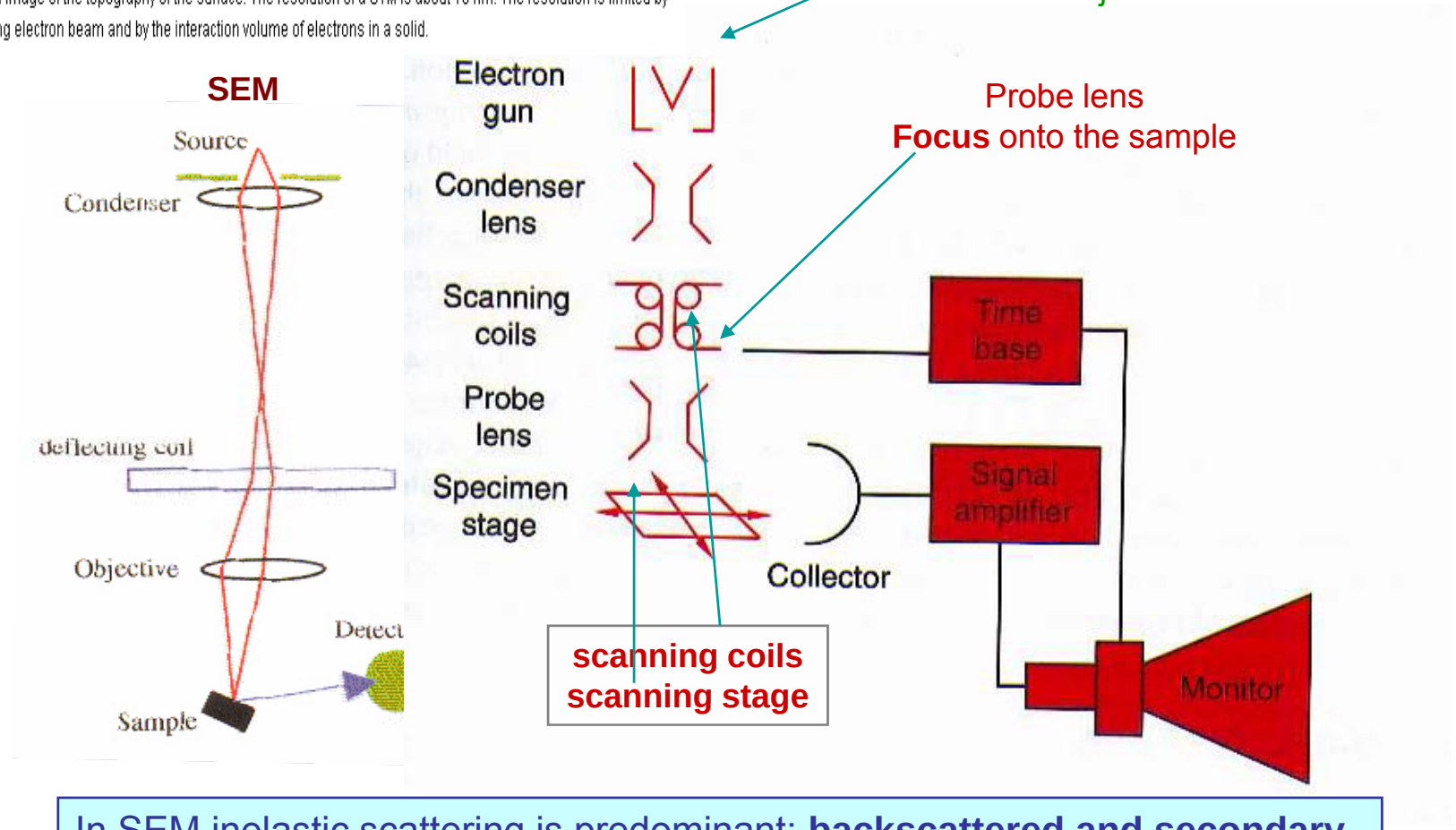

In SEM inelastic scattering is predominant: **backscattered and secondary electrons** as well as **X-ray photons** emitted from points at the sample surface (or slightly beneath) are collected and analyzed

SEM basics I

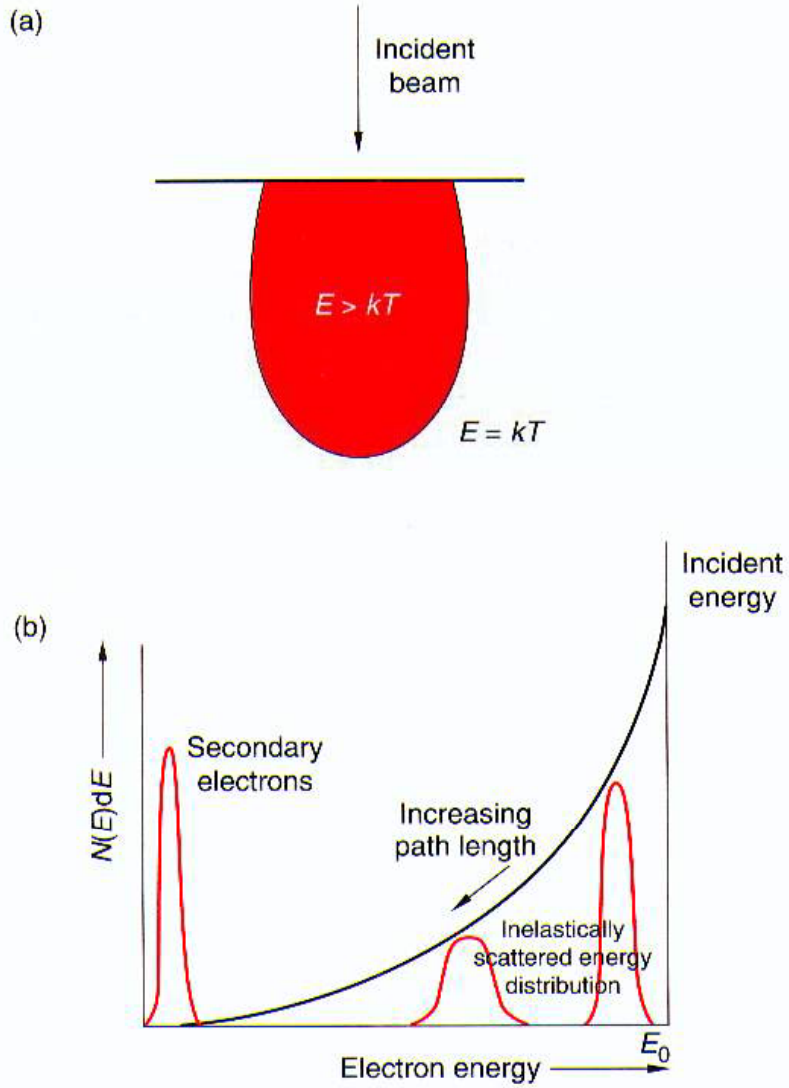

Figure 4.29 (a) The electron beam is inelastically scattered within an envelope bounded by the condition that the average energy has reached the thermal kinetic value kT. (b) The energy spread increases and the average energy of the electron falls as the path length within the solid increases (channelling effects and lattice anisotropy being ignored). (c) Random scattering models for individual electrons (Monte Carlo simulation) provide a vivid image of both the energy distribution and the spatial distribution of the electrons in the volume of the material beneath the beam, as well as the origin of the back-scattered electron signal

SEM does not require sample to be crossed by electrons:

→ Thick samples can be analyzed
→ Strong dependence on conductivity (dielectric samples must be metallized)
→ **Backscattered electrons** are collected
→ **Secondary electrons and X-rays photons** are produced (inelastic scattering)
→ Space resolution is lower than in TEM (contrast is based on less sensitive processes) and **is directly associated with the (focused) beam size**

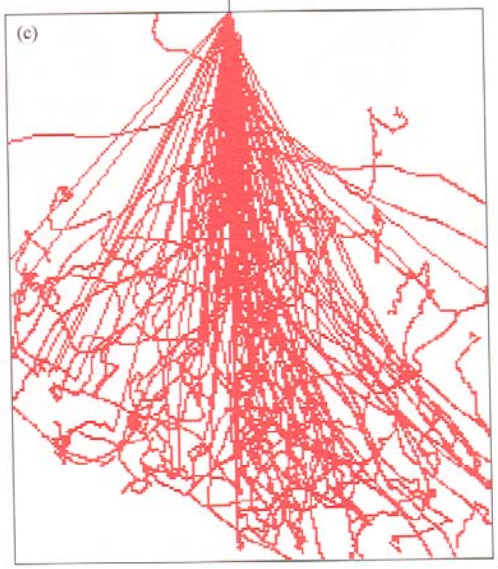

SEM basics II

Da Brandon Kaplan
Microstruct. Charact.
of Materials
Wiley (1999)

4.3.1.2 INELASTIC SCATTERING AND ENERGY LOSSES

The calculation of inelastic scattering paths can be accurately simulated by *Monte Carlo* methods, providing that some specifically *crystallographic* effects are ignored (for example lattice anisotropy and channelling processes along preferred directions). The electrons in the beam entering the crystal follow an irregular scattering path, losing energy as the path length in the crystal increases (Fig. 4.29). It is not possible to calculate any average trajectory for multiply scattered electrons, but it *is* possible to define (and measure) two critical depths, as well as to estimate the envelope which defines the boundaries of the electron trajectories for any given average energy. Thus, the *diffusion depth* x_D is defined as that depth beyond which the electrons are randomly scattered in all directions, so that an electron is equally likely to be scattered in any direction. At depths below x_D, there is a net drift of electrons towards increasing depths. The *penetration depth* or range, x_R, is defined as the depth at which the electron energy is reduced to the thermal energy kT. Both x_D and x_R *decrease* with *increasing* atomic number Z and *decreasing* incident beam energy E_0, but whereas the change with beam energy is more or less self-similar, that with atomic number is not. The shape of the envelope of scattered paths changes markedly with the atomic number, primarily because the lateral spread of the beam is roughly proportional to the difference $(x_D - x_R)$, while x_R is less sensitive to Z than x_D. These effects are summarized schematically in Fig. 4.30.

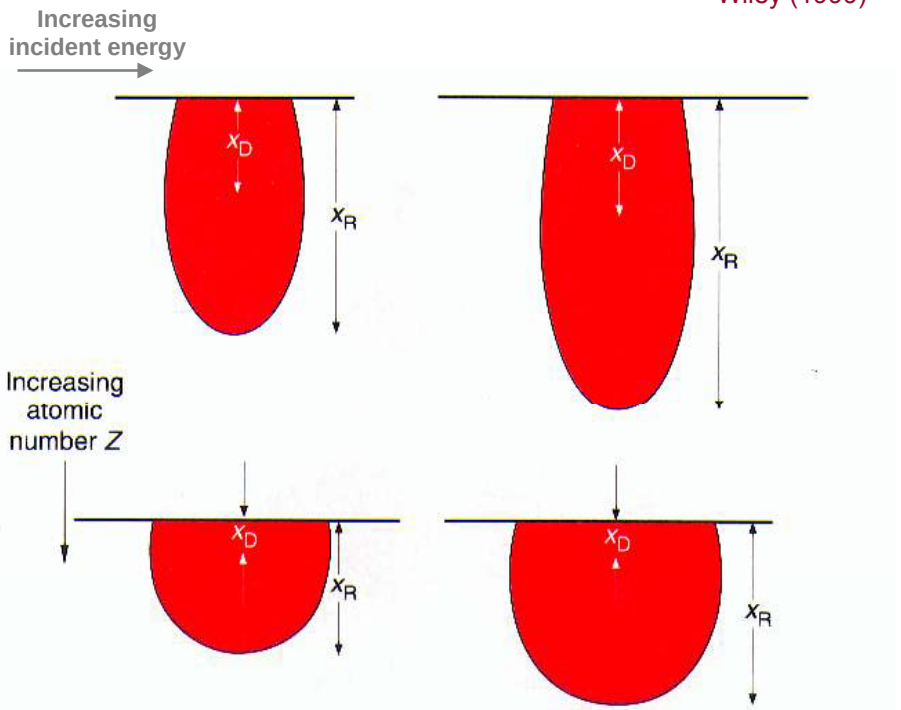

Figure 4.30 The inelastic scattering envelope for an incident beam of energetic electrons depends on both the incident energy and the atomic number of the target, and is qualitatively characterized by the two parameters, diffusion depth, and penetration depth (or range)

Scattering cross sections depend on the atom number Z ⇒ penetration length depends on Z, i.e., on the material under investigation

Electron penetration into the sample depends on the material properties *(basis for a contrast mech.)*

Microanalysis through X-ray emission

4.3.2 Electron Excitation of X-rays

If the incident electron energy *exceeds* the energy required to eject an electron from an atom in the specimen, then there exists a finite probability of such an *ionization event* occurring. *Ionization* of the atom occurs by an inelastic scattering event which raises the energy of the atom above the *ground state* by an amount equal to the ionization energy. The energy of the atom can then decay by an *electron transition* into the now vacant state. All such transitions are accompanied by the emission of a *photon*, and if the excited state of the atom corresponds to the ejection of an electron from one of the *inner shells* of the atom, then this photon will have an energy in the *X-ray* region of the spectrum.

In general, decay of an atom from the excited state takes place in more than one stage, with the emission of several photons of different wavelengths, each corresponding to a transition of the excited atom back towards the ground state. It follows that the energy lost by the incident electron *must* exceed the threshold energy for the ionization state if that particular ionization state is to be achieved, while the energy of the *most energetic* photon which can be emitted will always be *less* than this threshold for excitation. Furthermore, if we consider a particular inner shell of electrons (for example the innermost K-shell), then, as the atomic number increases the *ionization energy* for electrons occupying this shell must also increase (since the inner-shell electrons are more deeply embedded in the atom for the higher atomic numbers). An approximate representation of the situation is shown in Fig. 4.31.

The X-ray spectrum generated when an electron beam hits a solid target contains *all* wavelengths, starting from the *minimum* wavelength derived from the relationship $\lambda_0 = hc/eV$, where h is the Planck constant, c is the speed of light, e is the charge of the electron and V is the accelerating voltage applied to the electron beam (see Section 2.3.1).

The wavelengths of the *characteristic lines* which are emitted constitute *fingerprint* for the elements present in the solid and provide a powerful method of

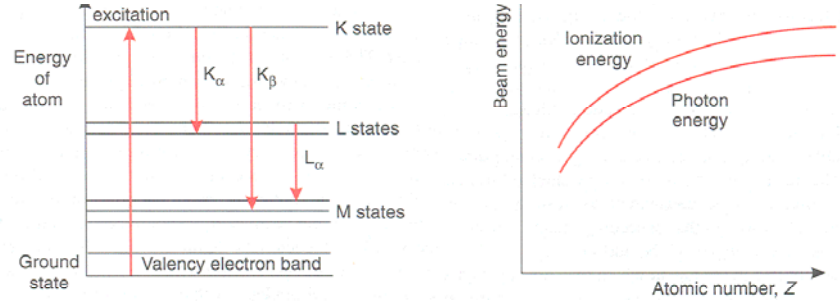

Figure 4.31 (a) An inelastic electron scattering event involving ionization of an inner-shell electron raises the energy of the atom to the appropriate ionization state, with subsequent decay to a lower energy being accompanied by photon emission. The photon emitted is characteristic of the energy difference between the two energy states, but must always be less than that required for ionization. (b) The ionization energy required to eject an electron from a particular inner shell increases with the atomic number

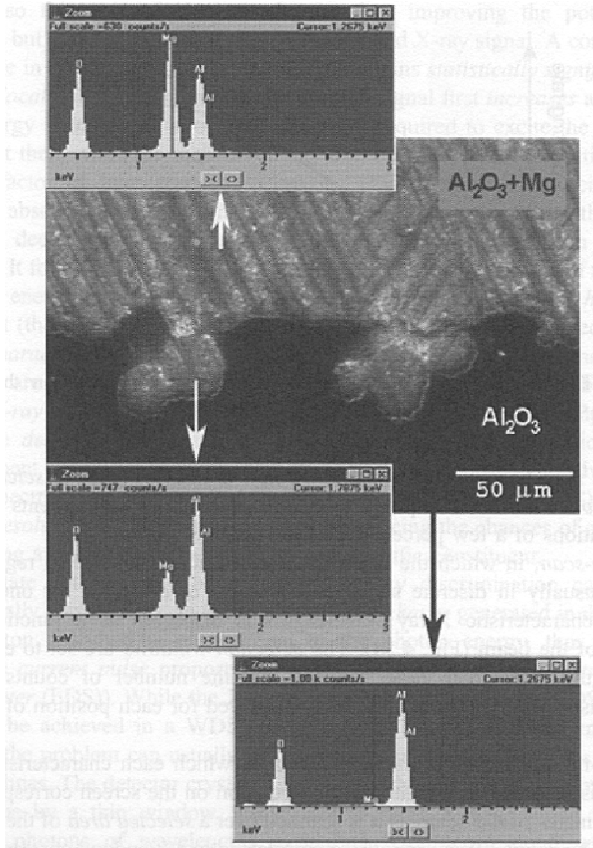

Figure 4.33 X-ray spectra obtained from a porous alumina specimen partially infiltrated with magnesium, showing the presence of oxygen, magnesium and aluminium in different regions of the microstructure via characteristic lines superimposed on a background of white radiation

Microanalysis methods can be readily implemented in SEM
(e.g.: X-ray Photoelectron Spectr. - XPS, Rutherford BackScattering - RBS, Secondary Ioniz. Mass Spectr. - SIMS, …)

Electron backscattering

4.3.3 Back-Scattered Electrons

A proportion of the incident electrons will be scattered by angles greater than π and may escape from the surface. The proportion of these *back-scattered* electrons, **R**, will depend on the *average atomic number* of the specimen but is almost independent of the incident beam energy. The back-scattered electrons originate in a *surface layer* corresponding to the diffusion distance and come from an area beneath the beam which is also proportional to this distance, but significantly less than the diameter of the envelope of inelastically scattered electrons.

The *average energy* of the back-scattered electrons is of course *less* than that of the primary incident beam, but nevertheless of the same order of magnitude. These electrons are usually detected in an annular region close to the probe lens pole-pieces. The collection efficiency is high, but the back-scattered electron current is only a fraction of the incident beam current.

4.3.3.1 Image Contrast in the Back-Scattered Image

Contrast in a *back-scattered electron image* may arise from either of the following two sources;

(a) Any region of the specimen surface which is tilted *towards* a back-scattered electron detector will give rise to an *enhanced* signal, while the signal will be *reduced* if the surface is tilted *away* from the detector. A segmented annular detector can therefore be used to obtain a *topographic image* of the surface in which the signals collected from *diametrically opposite detectors* are first subtracted and then amplified, thus enhancing differences in contrast from regions tilted in opposite directions.

(b) On the other hand, collecting a backscattered image from a *conical detector* surrounding the probe lens pole-pieces (or equivalently, *summing* the signals detected from all of the segments) will effectively *decrease* contrast associated with changes in surface topography. Most features detected in the image are then due to *atomic-number* contrast, and reflect variations in the density (usually the composition) of the sample.

The resolution in the *back-scattered electron* (BSE) *image* is typically an order of magnitude better than can be obtained from an *X-ray elemental map*, but not nearly as good as that available in the *secondary electron image* (discussed below). The direct relationship between the BSE image and the *diffusion distance* in the material typically results in a resolution of the order of 10–20 nm when working at 10–20 kV. The BSE image can give very useful information on the *distribution* of the phases present, providing that they differ sufficiently in density (see Fig. 4.36), if the secondary electron image is lacking in contrast.

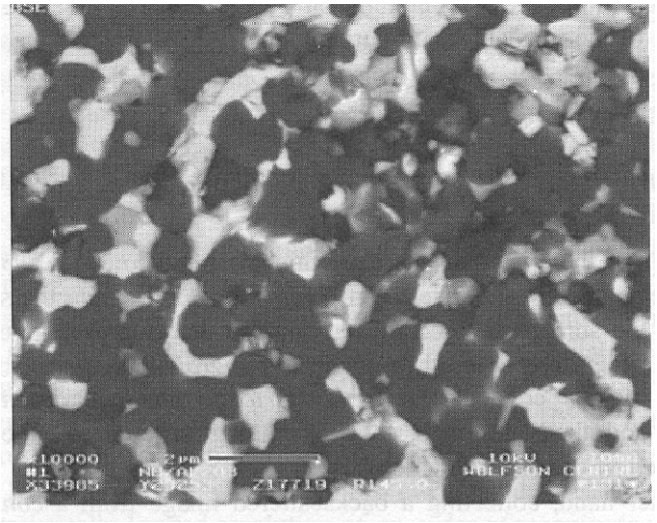

Figure 4.36 Back-scattered electron–atomic number contrast image showing a niobium-rich intermetallic phase (bright contrast) dispersed in an alumina matrix (dark contrast)

(Convoluted) **topographical / compositional** images can be achieved by collecting backscattered electrons

Typ max space resolution ~ 10 nm (due to the “buried” origin of the backscattered electrons) at 20 keV electron energy

Secondary electrons

4.3.4 Secondary Electron Emission

Most of the electron current generated in a sample due to the impact of a high-energy incident beam is due to the release of *secondary electrons* from the surface. In fact, the *secondary electron emission coefficient*, the number of secondaries released per incident high energy electron, is *always* greater than one and may reach values of several hundred. All of these secondaries have rather similar energies, up to 100 or 200 eV, but typically in the range 10–50 eV, and they are therefore readily deflected by a low-bias voltage and collected with very high efficiency (close to 100 %). Moreover, their low kinetic energy severely restricts their mean free path in the sample, so that the secondaries escaping from the surface are generated very close to the latter, typically within 1–2 nm, and are almost unaffected by beam spreading beneath the surface.

Four factors directly affect *secondary emission* from the surface:

(a) The *work function* of the surface, that is the energy which has to be supplied t an electron in the solid which is at the *Fermi level*, in order to permit it to escap from the surface. Typical work functions are a few eV in magnitude, with th work function depending on both the *composition* and the *atomic packin* (crystal structure) at the surface. The work function is sensitive to both *surfac adsorption* and films of *contamination*.

(b) The *beam energy* and *intensity*. As the beam energy is increased, mor secondaries might be expected to be created, but a high-energy beam i inelastically scattered further beneath the surface, so that the *proportion* c secondaries escaping from the surface is reduced. On the other hand, th secondary electron current is *directly proportional* to the current in the incide beam.

(c) The *density of the sample* has a relatively limited influence, and is usuall masked by the effect of surface films or surface contamination. Since highe atomic-number materials have a smaller diffusion distance, the number of hig energy electrons is higher in the surface region for any given beam intensity, th *increasing* the number of secondaries. This effect is most pronounced at *lo* beam energies, when the diffusion distance is comparable to the mean free pa of the secondary electrons.

(d) The most pronounced effect is that of *surface topography*, or more precisely, t local *curvature* of the surface. Any region protruding from the surface (*positi* radius of curvature) improves the chances of secondaries escaping, while a

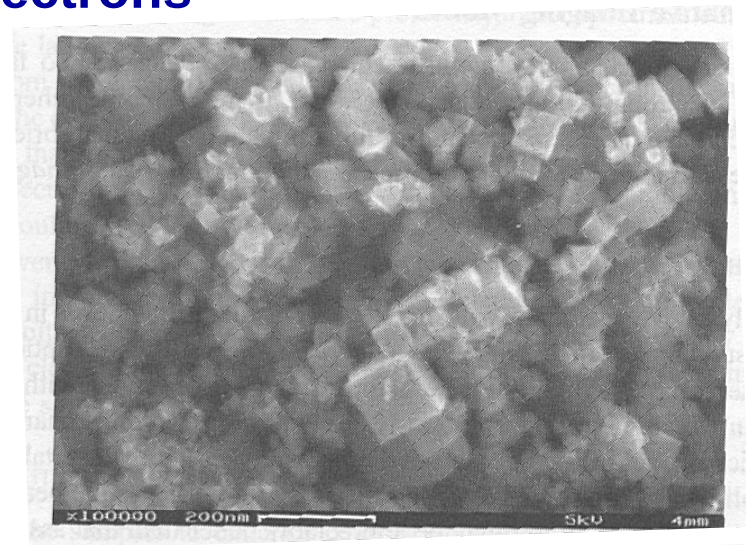

Figure 4.38 A high-resolution secondary electron image of nano-sized TiCN particles

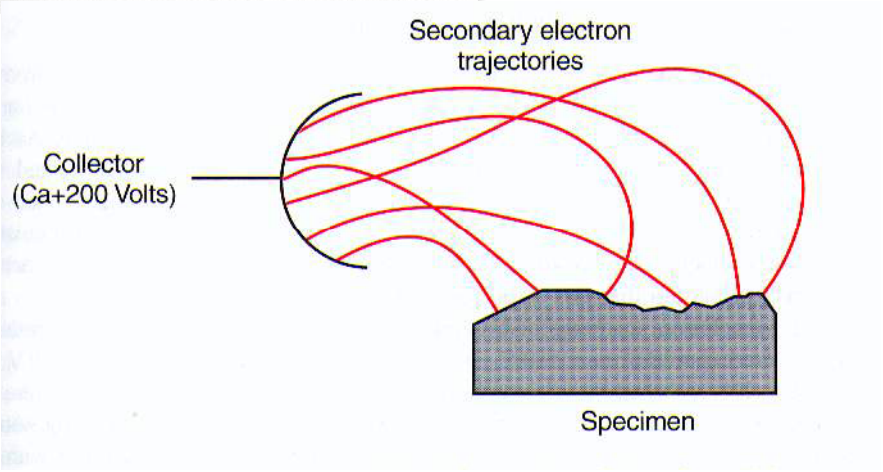

Higher space resolution (limited by the electron beam size) can be achieved with secondary electron collection

Electron optics in SEM and EBL

Tight focussing of the beam (down to **1-5 nm**) essential to achieve space resolution in SEM (and EBL!) ⇒ electron optics rules the ultimate space resolution

Spherical aberration

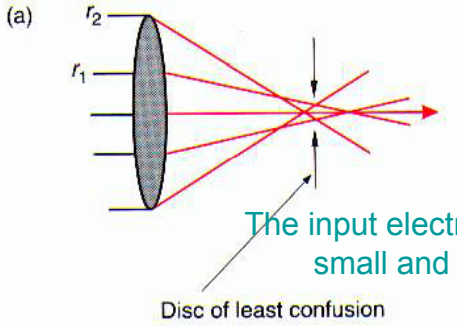

The input electron beam should be small and well collimated

Chromatic aberration

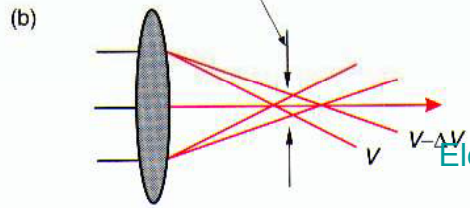

Electron energy must be well controlled

Figure 4.4 Spherical (a) and chromatic aberration (b) prevent a parallel beam from being brought to a point focus. Instead, a disc of least confusion is formed in the focal plane

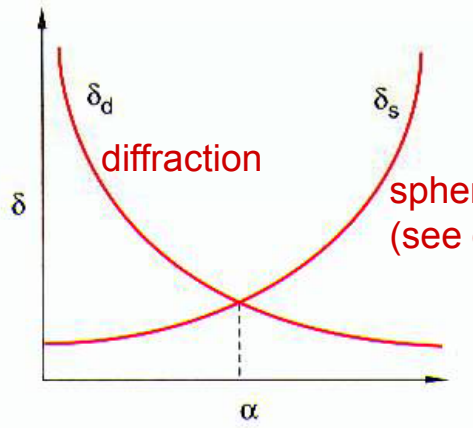

Figure 4.5 The diffraction and the spherical aberration limits on resolution have an opposite dependence on the angular aperture of the objective, so that an optimum value of α exists

Charge acceleration (i.e., energy) helps in achieving collimation of the beam, hence to access a more efficient optics

Spherical aberration can be relevant enhanced by Coulomb self-repulsion of electrons (for bright beams)

Obtaining a bright and well focused electron beam, able to approach the diffraction limit, is a technical challenge

Issues in EBL beam conditioning I

Spherical Aberration

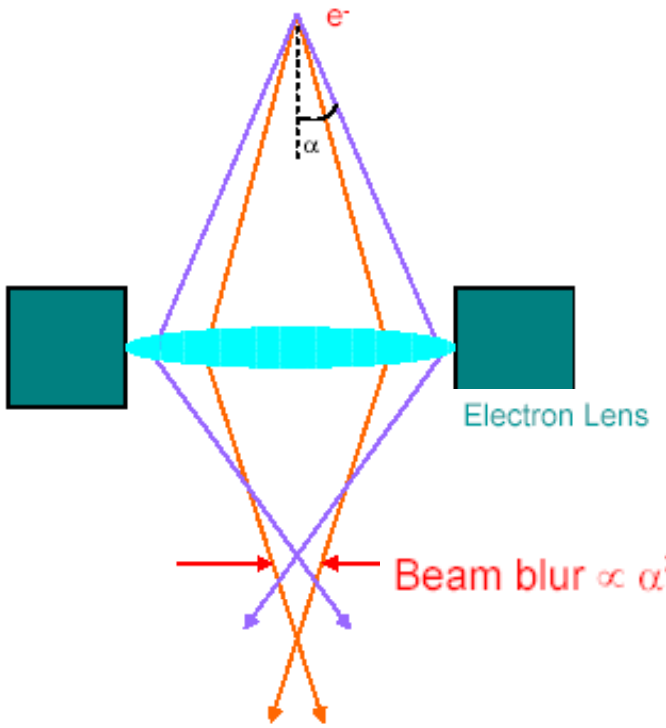

Coulomb Interaction

Boersch Effect

- Electrons repel each other in the beam direction
  Causes energy spread among electrons
- Result in chromatic aberration

Loeffler Effect

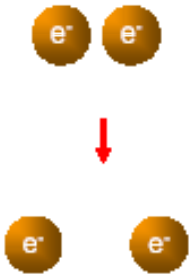

- Electrons repel/collide each other in the radial direction
- Causes trajectory change and energy spread among electrons
- Result in chromatic as well as spherical aberration

Electron optics pose additional problems with respect to conventional optics

High electron energy needed to achieve focusing

3. Writing patterns with electron beams

5.1 Electron Beam Direct Write

In electron beam direct write electrons are formed to a beam and are accelerated to a determined position on the wafer surface, where the resist has to be exposed to form the pattern. An electron beam system consists of the electron source or electron gun, the electron-optical system (the electron column), a mechanical wafer stage and a controller system. A schematic view of an electron beam lithography tool is given in Figure 18.

The two types of electron guns which are commonly used are thermionic sources, on the one hand, and field emission sources, on the other hand. In thermionic sources the electrons are emitted by heating the source material, such as tungsten (W) or lantanum hexaboride (LaB_6). While LaB_6 offers a higher brightness (10^5(A/cm^2)/steradian)) and a longer lifetime (~1000 h) than W (10^4(A/cm^2)/steradian; ~100 h), W has the advantage that vacuum requirements are not as high as for LaB_6. Nevertheless, LaB_6 has become the standard source for thermionic e-beam sources.

In field emission sources the electrons are extracted from a sharp tip by a high electric field. Though these sources have a high brightness (10^7(A/cm^2)/steradian)), they are unstable and require a ultrahigh vacuum. Therefore they have not been widely adopted in electron beam lithography systems.

In the electron column the extracted electrons are formed to a beam with a definite diameter or shape. Therefore different electron-optical elements as focusing and defocusing lenses and apertures are employed. Further parts of the column are a beam blank to switch the beam on and off and a beam deflection system, with which the beam is positioned on the wafer.

Since the deflection system can only address a field of 400 – 800 µm (depending on spot size and tool), it is necessary to move the sample under the beam from one exposure field to the next by a mechanical wafer stage. The position of the stage is measured by an interferometer, so it is possible to adjust the beam with an accuracy of ~5 nm.

The whole system has to be under vacuum to enable the electron beam to be formed and has to be isolated from vibrations. Further requirements are low electromagnetic stray field, because this would hamper the positioning of the beam.

The pattern, which is given as a CAD file, is translated into movements of the electron beam/wafer stage by a computer. During an illumination, the tilt of the sample is measured continuously and the focus is adjusted. There are two exposure schemes: In the first one, the raster scan scheme, the deflection system and the wafer stage address every point of the sample, but the beam is switched on and off according to the structure. In the second scheme, the vector scan scheme, only the points which have to be illuminated are addressed. Hence the vector scan scheme is less time-consuming than the raster scan scheme.

The time needed for the illumination of a whole wafer depends on the pattern, but because the electron beam direct write is a serial method, it is time-consuming and not suitable for the industrial mass production of microelectronic circuits. Nevertheless, because the resolution is pushed to a few nanometers, it has a high impact on research activities and is the method of choice for defining the pattern on the masks used for optical lithography.

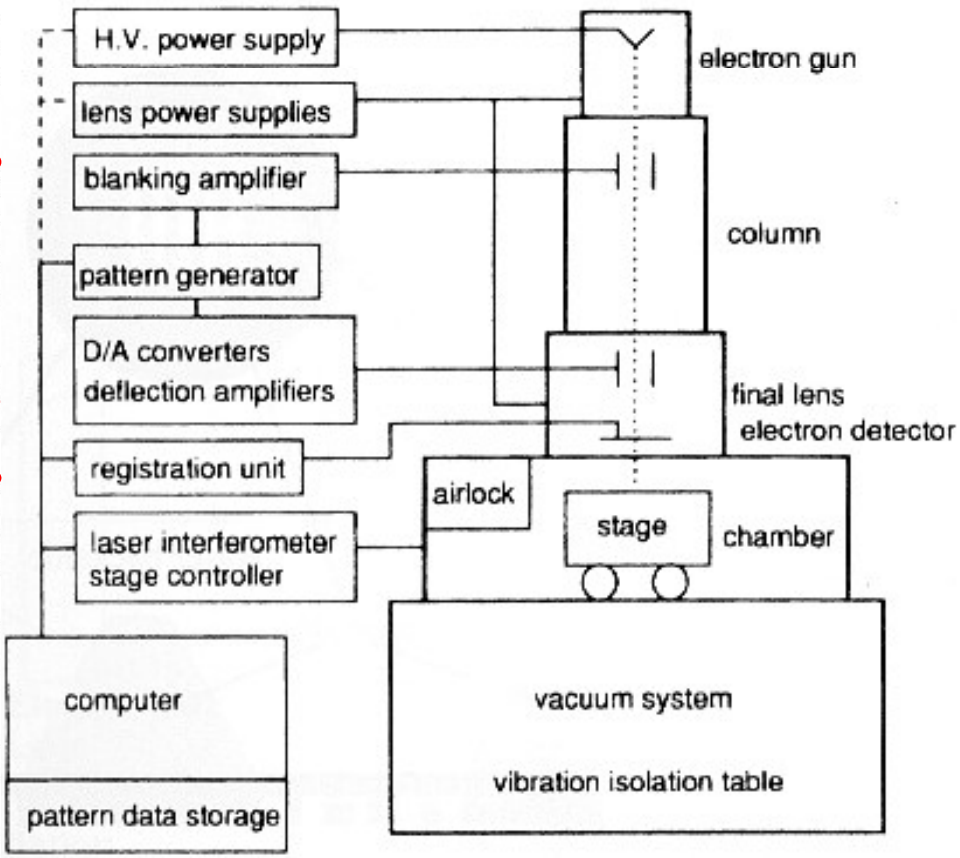

The electron beam of a SEM can be used to “write” an arbitrary pattern onto a surface

Electron Beam Lithography (EBL)

Accelerated charged particles can be used for:
- etching, milling etc. (better with heavy ions, see FIB)
- **resist impression** (*true* electron beam lithography)

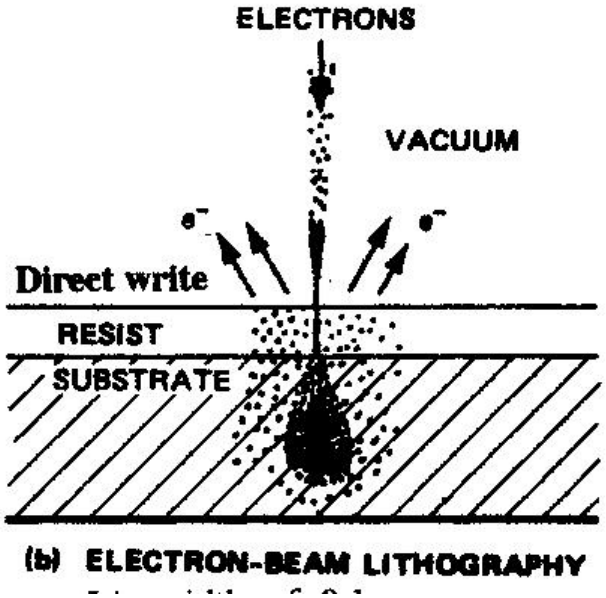

TABLE 1.6 Electron- and Ion-Beam Applications

Electron-Beam Applications	Ion-Beam Applications
Nanoscale lithography	Micromachining and ion milling
Low-voltage scanning electron microscopy	Microdeposition of metals
Critical dimension measurements	Maskless ion implantation
Electron-beam-induced metal deposition	Microstructure failure analysis
Reflection high-energy electron diffraction (RHEED)	Secondary ion mass spectroscopy
Scanning auger microscopy	

Da Madou, Fundamentals of microfabr. CRC (1997)

Excellent space resolution (similar to SEM/TEM, i.e., below 10 nm)

Pros and cons of EBL

- Diffraction is not a limitation on resolution
- Resolution depends on beam size, can reach ~ 5 nm
- Two applications:
  - Direct Writing
  - Projection (step and repeat) ??
- Issues:
  - Throughput of direct writing is very low – research tool or low pattern density production
  - Projection stepper is in development stage (primarily by Nikon). Mask making is the biggest challenge for projection method
  - Back-scattering and second electron result in proximity effect – reduce resolution with dense patterns
  - Operate in high vacuum (10-6 – 10-10 torr)

Space resolution in EBL

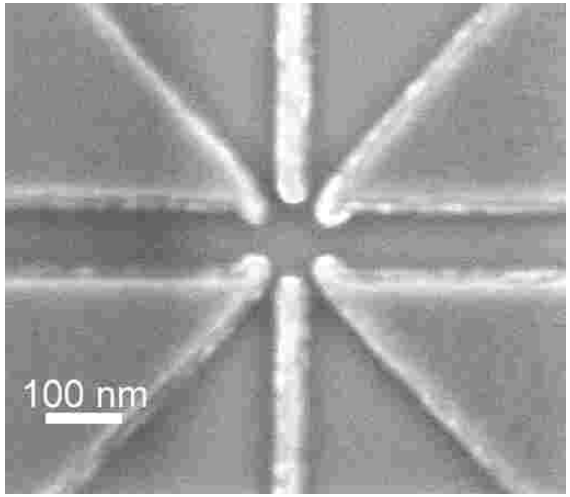

Ti/ Al gate structures for a SET device generated by e-beam lithograph and lift-off.

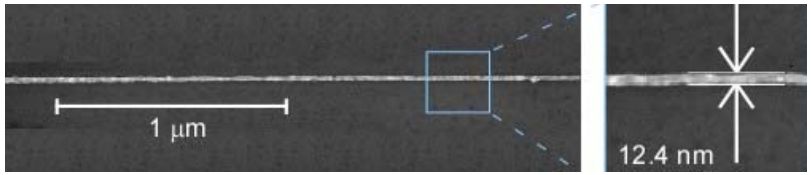

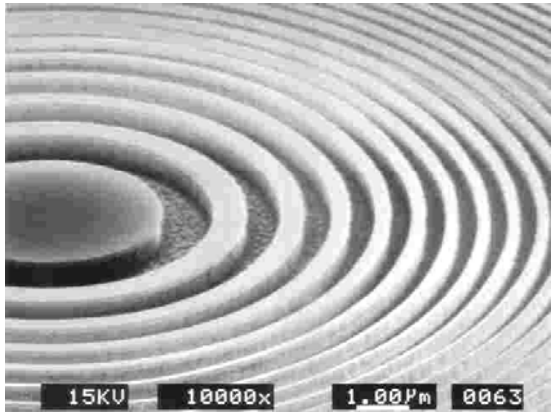

A Bragg-Fresnel lens for x-rays exposed in continuous path control mode and etched into Si.

This is an SEM image of a lifted off wire that has a width of ~12 nm. The line was written in 70 nm PMMA and metallized with Ti(10 nm)/Au(20 nm). The work was performed at the Centre for Quantum Computer Technology, UNSW, Sydney, Australia.
Note that when making features on this size scale, the grain size of the metal using during liftoff becomes extremely important. For example, if the line width is smaller than the grain size of the metal, it will be impossible to produce a smooth line.

The resolution of an electron lithography system may be constrained by technological factors other than diffraction, such as *electron scattering* in the resist, *resist swelling*, and by various *aberrations* in the electron optics system

http://lmn.web.psi.ch/mntech/ebeam.htm
http://www.siliconfareast.com/lith_electron.htm
http://www.jcnabity.com/

Issues in EBL beam conditioning II

Beam Size (d)

$$d = \sqrt{d_g^2 + d_s^2 + d_c^2 + d_d^2}$$

The angular spread α of the beam plays a role similar to the acceptance angle (numerical aperture) in convenitional microscopy

$$d_g^2(Virtual\ \ Source) = \frac{d_v}{M}$$

(d_v - Source size, M – demagnification)

$$d_s^2(Spherical\ \ Aberration) = \frac{1}{2} C_s \alpha^3$$

(C_s – spherical aberration, α – beam convergence angle

$C_s \propto$ f (focal length))

$$d_c^2(Chromatic\ \ Aberration) = C_c \alpha \frac{\Delta E}{V_b}$$

(C_c – chromatic aberration, ΔE – electron energy spread, V_b – electron acceleration voltage)

$$d_d^2(Diffraction\ \ Limit) = 0.6\frac{\lambda}{\alpha}$$

$$\lambda = \frac{1.2}{\sqrt{V_b}}(nm)$$ (electron wavelength

For High Resolution:

↗ M, ↗ V_b, ↘ ΔE, ↘ f

What about α?

Resolution vs. Convergence Angle

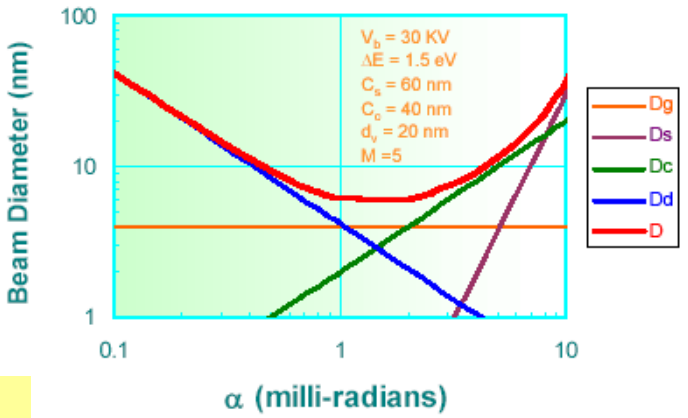

Typically, minimum beam size is in the few nm range

DOF = d / α

Resist issues in EBL

Advantages:

* Computer-controlled electron beam
* No mask is needed
* Can produce features well sub-1 μm (for instance, masks for optical lithography!)
* Diffraction effects are minimized
* Electron beam can detect surface features for very accurate registration

Disadvantages:

* *Swelling occurs when developing negative electron beam resists*, limiting resolution
* Expensive as compared to light lithography systems
* Slower as compared to light lithography systems
* *Forward scattering in the resist and back scattering in the substrate limit resoution*

http://web.cecs.pdx.edu/~jeske/litho/electronbeamlitho.html

Resist swelling occurs as the developer penetrates the resist material. The resulting increase in volume can distort the pattern, to the point that some adjacent lines that are not supposed to touch become in contact with each other.

Resist contraction after the resist has undergone swelling contraction can also occur during rinsing. However, this contraction is often not enough to bring the resist back to its intended form, so the distortion brought about by the swelling remains even after rinsing. Unfortunately, a swelling/contraction cycle weakens the adhesion of the smaller features of the resist to the substrate, which can create undulations in very narrow lines. **Reducing resist thickness** decreases the resolution-limiting effects of swelling and contraction.

Resists for EBL

Organics (e.g., PMMA) or inorganics thin films (e.g., fluorides, amorphous calchogenides, AsS, AsSe,… acting as negative resists)

When electrons strike a material, they penetrate the material and lose energy from atomic collisions. These collisions can cause the striking electrons to 'scatter', a phenomenon that is aptly known as 'scattering'. The scattering of electrons may be backward (or back-scattering, wherein electrons 'bounce' back), but it is often forward through small angles with respect to the original path.

During electron beam lithography, scattering occurs as the electron beam interacts with the resist and substrate atoms. This electron scattering has two major effects: 1) it broadens the diameter of the incident electron beam as it penetrates the resist and substrate; and 2) it gives the resist unintended extra doses of electron exposure as back-scattered electrons from the substrate bounce back to the resist.

Thus, scattering effects during e-beam lithography result in wider images than what can be ideally produced from the e-beam diameter, degrading the resolution of the EBL system. In fact, closely-spaced adjacent lines can 'add' electron exposure to each other, a phenomenon known as 'proximity effect.'

Technological problem of EBL: Resist material (especially negative)

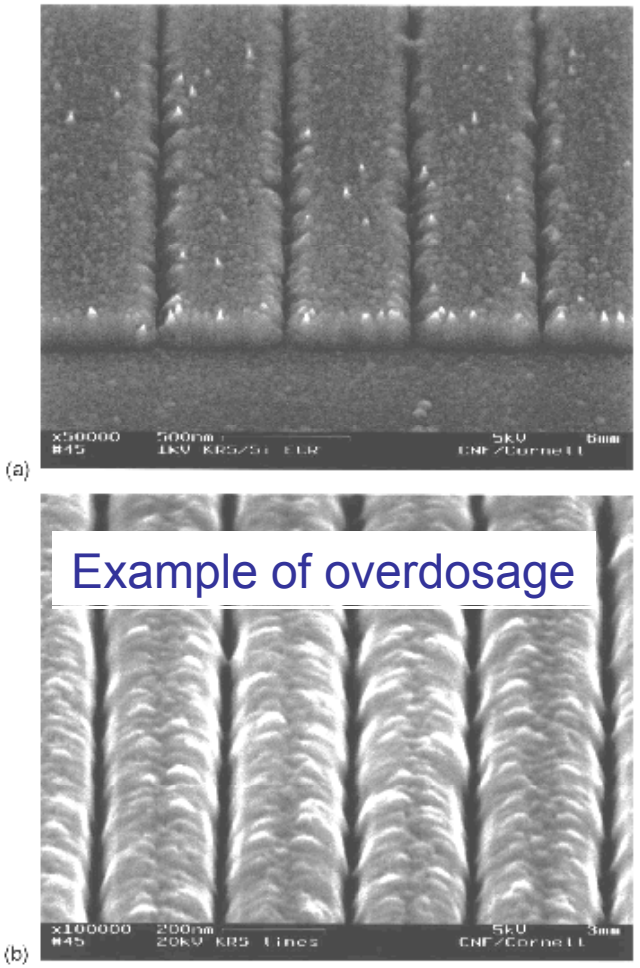

FIG. 3. Single pass lines etched into Si using the two step ECR etch, for KRS resist exposed at 1 keV (a) and a 20 keV (b) with line doses of 11 and 175 pC/cm, respectively.

Backscattering problems

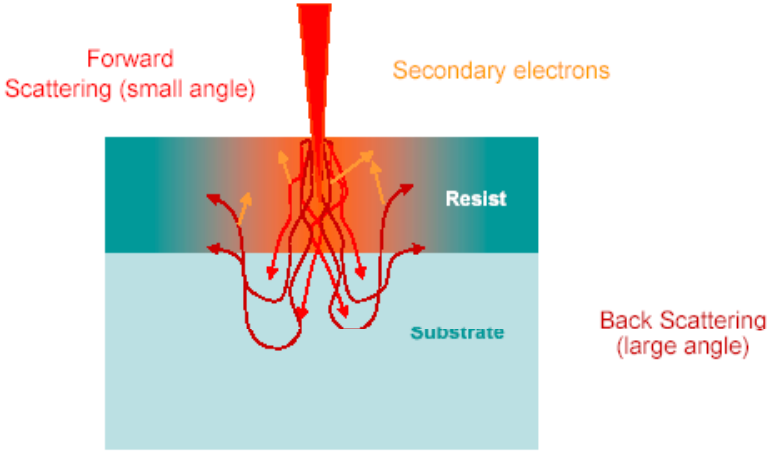

The scattered electrons also expose the resist!

Scattering Energy Distribution

Double Gaussian Distribution

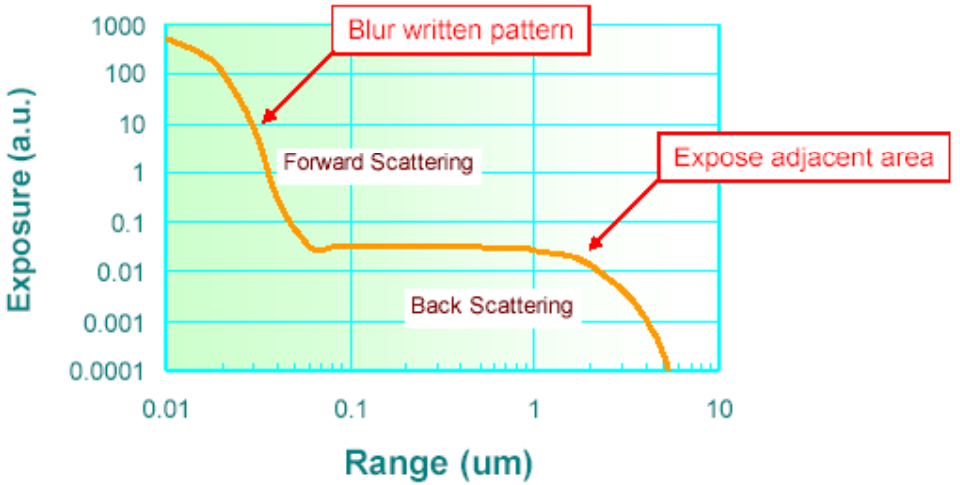

Proximity Effect

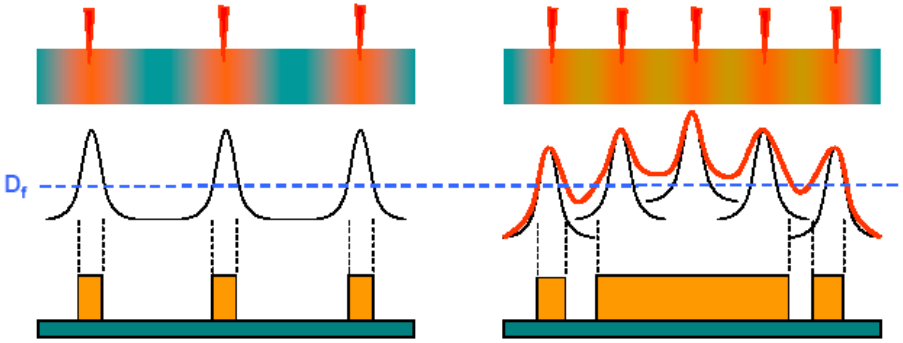

MTF is greatly reduced at high pattern density

Resist impression difficult to control (completely) because of high electron energy

How to achieve the best resolution: a vivid example I

IEEE TRANSACTIONS ON NANOTECHNOLOGY, VOL. 4, NO. 3, MAY 2005

High-Resolution Electron Beam Lithography and DNA Nano-Patterning for Molecular QCA

Wenchuang Hu, *Member, IEEE*, Koshala Sarveswaran, Marya Lieberman, and Gary H. Bernstein, *Senior Member, IEEE*

***Abstract*—Electron beam lithography (EBL) patterning of poly(methylmethacrylate) (PMMA) is a versatile tool for defining molecular structures on the sub-10-nm scale. We demonstrate lithographic resolution to about 5 nm using a cold-development technique. Liftoff of sub-10-nm Au nanoparticles and metal lines proves that cold development completely clears the PMMA residue on the exposed areas. Molecular liftoff is performed to pattern DNA rafts with high fidelity at linewidths of about 100 nm. High-resolution EBL and molecular liftoff can be applied to pattern Creutz–Taube molecules on the scale of a few nanometers for quantum-dot cellular automata.**

In general, "top-down" lithographic methods have difficulties in satisfying the requirements of both resolution and throughput. On the other hand, self-assembly has shown the capability for patterning nanocomponents, such as nanoparticles

EBL is performed using our 30-kV cold-cathode field emission Hitachi S-4500 scanning electron microscope converted to EBL [12]. The spot size is about 1 nm. One advantage of using this system is the ease of achieving optimum beam parameters prior to exposure, assuring that the best possible lithography results can be reliably achieved. We have used this system to investigate the effects of varying the developer temperature on ultimate lithographic resolution, and found that cooling the developer yields noticeable advantages.

For EBL, 30–70 nm, 950 K amu PMMA was used as a positive resist. Isopropyl alcohol: methyl isobutyl ketone (3 : 1) with 1.5 vol % methyl ethyl ketone was used as developer because of its high contrast [13]. During development, 10 ml of developer was cooled to the desired temperature of 4 °C to 8 °C with a precision of 1 °C. Development time varied from 30–90 s depending on the resist thickness (30–80 nm) and developer temperature (4 °C to 8 °C). Resist patterns were coated with 1–2-nm Cr or $Au_{60}Pd_{40}$ by an Emitech model 660 plasma sputter coater or a Varian thermal evaporator for SEM examination.

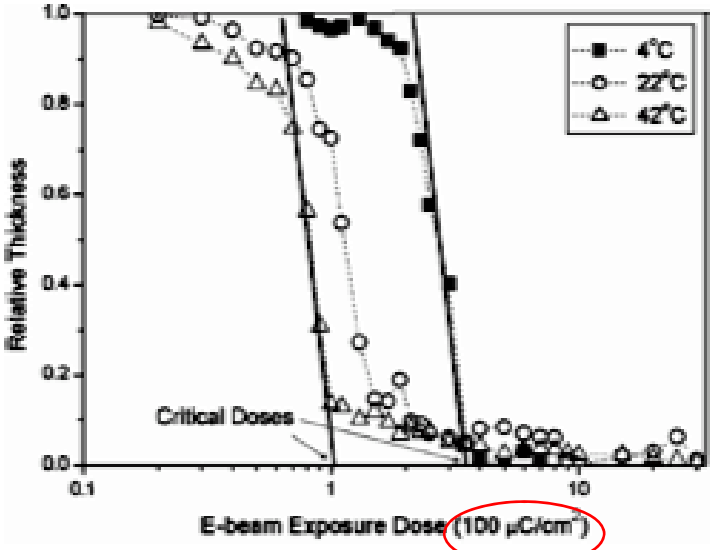

Fig. 1. PMMA contrast curves at development temperatures of 4 °C, 22 °C, and 42 °C, measured by AFM metrology.

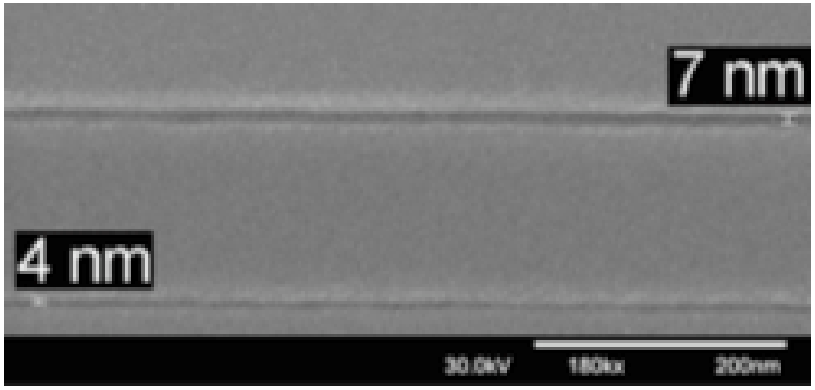

Fig. 2. 4–7-nm PMMA trenches sputter-coated with 2-nm Cr developed by cold development.

A vivid example II

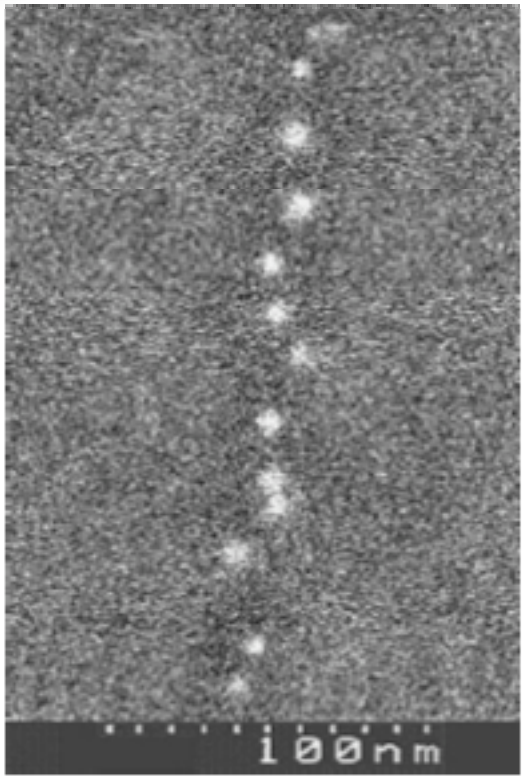

Fig. 4. Lifted-off line with one 5-nm Au nanoparticle in the width. The flow of nanoparticles to the edges of trenches caused the spreading of line.

Liftoff is nearly the only way to transfer high resolution of EBL from PMMA due to its poor etch resistance. For sub-10-nm liftoff, the most important issue is that the bottom of the narrow trenches must be clean of resist residue. To test the existence of resist residue in the trenches after cold development, we deposited 5-nm negatively charged gold nanoparticles [15] into the positively charged trenches (trench bottom was coated with polylysine after development). PMMA was then removed by dichloromethane (CH_2Cl_2) [16]. As can be seen in Fig. 4, a line of single particles is obtained, which would not be possible without a clean oxide surface at the bottom of the trench since the particles do not stick to PMMA residue. This result also demonstrates an example application of EBL to pattern sub-10-nm structures. These nanoparticle structures can be used for single electron devices [17], [18].

(Regular) nanoparticles formation

Nanolines formation

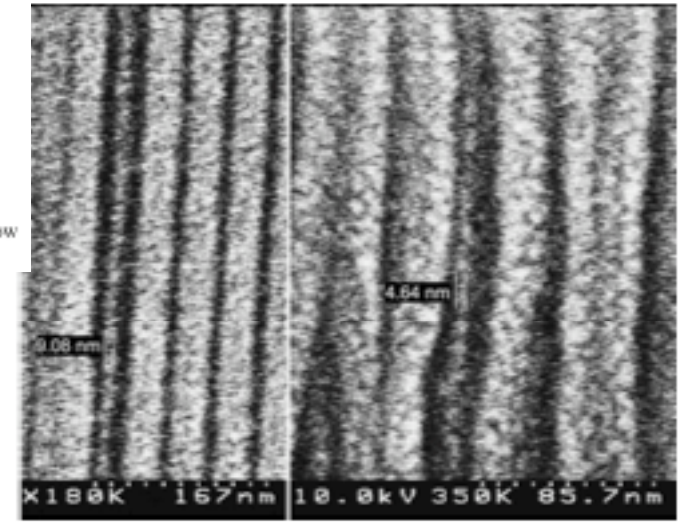

Fig. 5. $Au_{60}Pd_{40}$ lines (3 nm thick) with 5–10-nm width formed in 40-nm-deep PMMA trenches after PMMA removal. Formation of 5-nm lines proves complete development of narrow PMMA trenches by the cold-development technique.

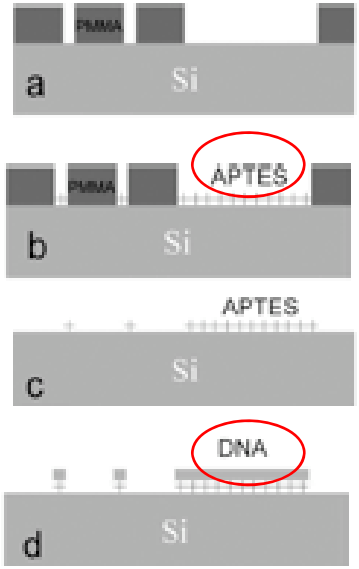

The (targeted) final resullt: “molecular lift-off”

The SCALPEL technique

5.2 SCALPEL

The drawback of electron beam direct write is the serial character of the method. In mass production, where throughput is concerned, exposure times of several hours are not acceptable. Though there are electron optics which could enable projection lithography analogously to optical projection lithography, this method suffers from the huge penetration depth of electrons. The masking layers have to be thick to stop a significant part of the electrons.

One method of circumventing this problem is the SCALPEL method (scattering with angular limitation in projection electron beam lithography). In SCALPEL a broad beam of electrons, 2 to 3 mm in diameter, is scanned across a mask consisting of a silicon-nitride membrane layer (~100 – 150 nm), on which a patterned scattering layer (25 to 50 nm of gold or tungsten) is situated (Figure 20a). The electrons, which only strike the membrane layer, will pass this layer mostly unscattered, while the electrons, which strike the scattering layer, will be distracted strongly from their path. The unscattered electrons are focused through an aperture and projected onto the wafer, while the scattered electrons will be blocked. So a high contrast image can be achieved.

As a projection lithography method, SCALPEL offers the advantage of image reduction thus making mask fabrication easier. The mask itself consists of silicon struts, between which the membrane layer is clamped (Figure 20b). The width of the membrane corresponds to the diameter of the electron beam, while it is a few cm in length. By means of the projection optics behind the aperture the electrons coming from two different membrane areas separated by a silicon strut can be stitched together at the wafer, so circuits of 2 cm times 3 cm can be exposed.

Attempts to overcome the limitations of a scanning technique with a "beam projection" approach

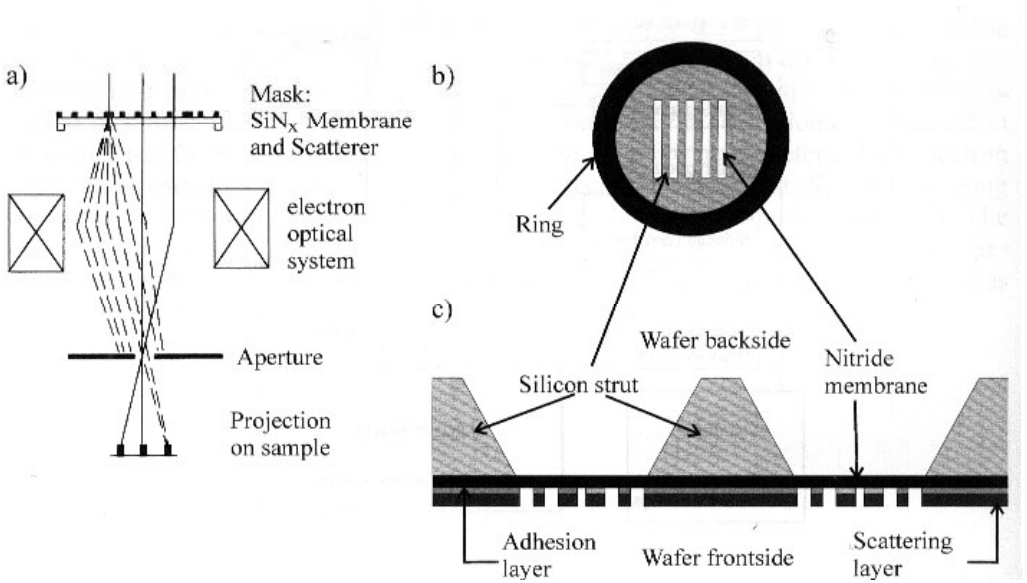

Figure 20:
(a) Electron path through a SCALPEL tool. A parallel beam of electrons passes through the mask; a scattering layer in which the pattern is inscribed scatters the electrons, so that they are not focused through an aperture by the electron optical system; only the unscattered electrons will pass the aperture. These electrons are projected onto the sample [16], [43].
(b) Top view of a mask and
(c) cross-sectional view of the mask. The masks are strips and separated by silicon struts. The masks are illuminated in series and the pictures of the masks are projected onto the adjacent sample .

“Maskless” electron projection

PML2 – Projection Mask-Less Lithography IMS Nanofabrication

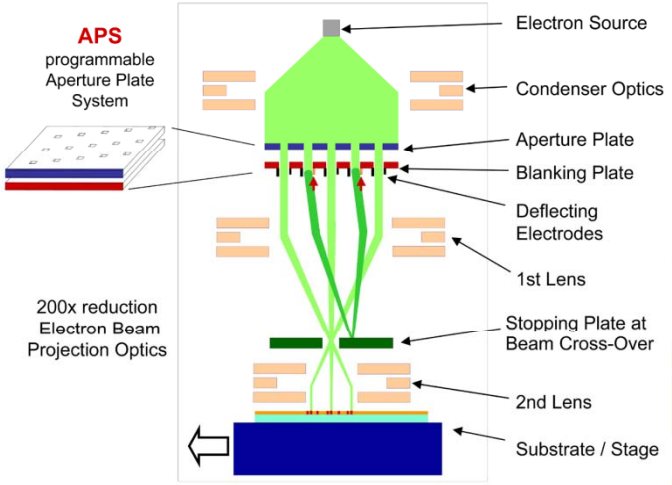

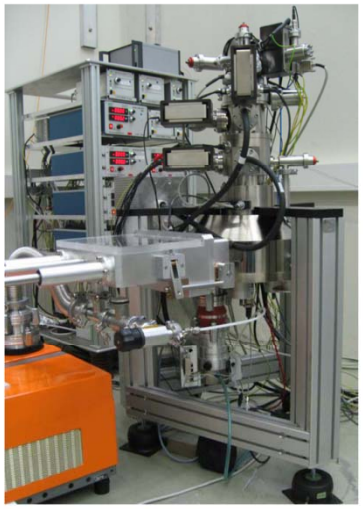

RIMANA European project / www.rimana.org

PML2 proof-of-concept system

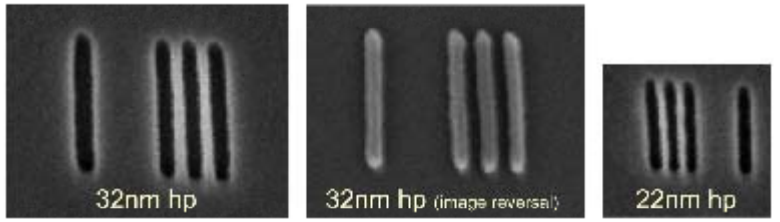

Figure 2. *The PML2 proof-of-concept system resolved lines with a half-pitc (hp) as small as 22nm, using poly-methyl-methacrylate (PMMA) resist.*

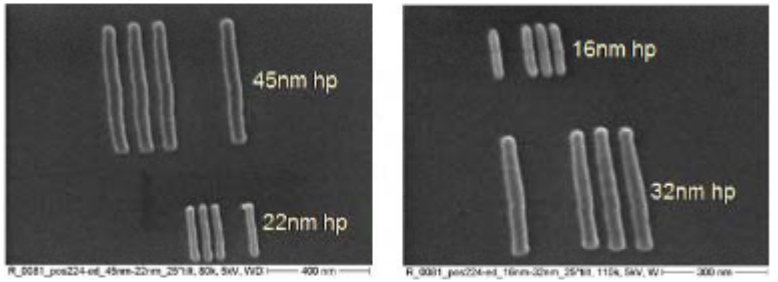

Figure 3. *The system printed lines in 50nm-thick hydrogen-silsesquioxane (HSQ) resis with a half-pitch as small as 16nm.*

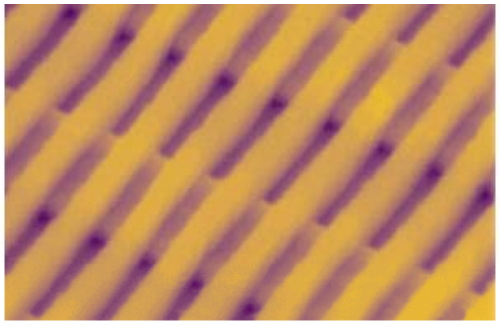

Magnified 35,000 Times

The tiny lines on this silicon wafer were created using Lucent's SCALPEL electron beam lithography. The right-leaning lines are .08 microns wide. It would take 1,250 of them to equal the width of one human hair. (Image courtesy of Lucent Technologies.)

Optimistic forecasts!!

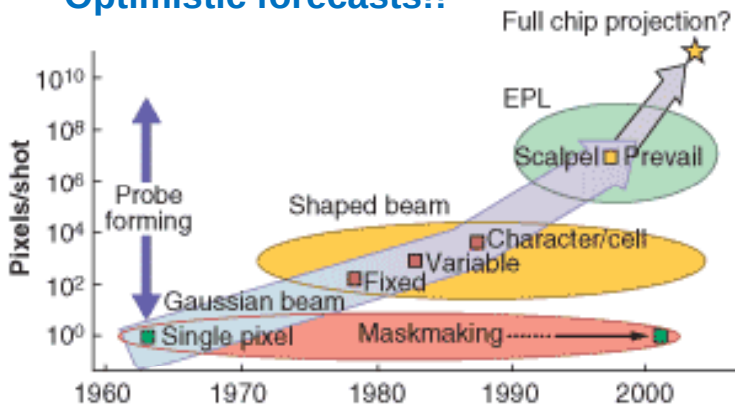

Focused Ion Beam (FIB)

6.1 Focused Ion Beam

The setup of a focused ion beam (FIB) tool is similar to an electron beam lithography tool, but instead of an electron beam a focused ion beam is used either to expose a resist locally, as in electron beam lithography, or to modify the substrate directly. The heavy ions impinging on the surface will sputter the material or, depending on energy, will intermix the layers at the surface of the sample. By means of this so-called ion milling the properties of the material at the surface will be altered. Another possibility is the local deposition of an additional layer. The impinging ions can induce the decomposition of a gas. As in a Chemical Vapor Deposition (CVD) process, where the decomposition of the process gasses is induced globally by thermal activation (Low Pressure CVD) or by a plasma (Plasma Enhanced CVD), this local decomposition leads to a local deposition of the material.

Besides a certain impact on the structure definition in the research environment, the direct modification of the surface, the sputtering as well as the deposition, enables the method to be used in the most important application of FIB in industry, namely mask repair. Mask production is very expensive and due to some failure in the processing (e.g. dirt sticking on the mask or a mistake in the electron beam pattern generator) a mask can be faulty. Either some parts of the masking layer, which should have been removed, are still present, or some parts of the masking layer are removed in excess. These faults can be cured by FIB.

Focused ion beams (accelerated) can be used as well (typ., for nanomachining)

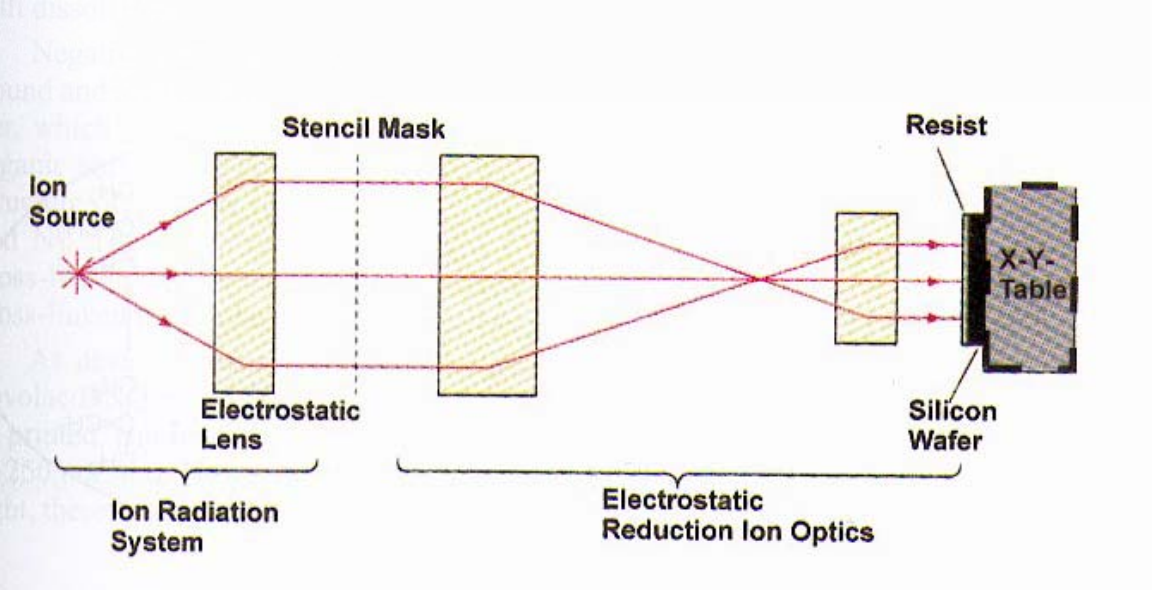

Figure 21: Schematic view of an ion projection lithography tool.

Realization of FIBs

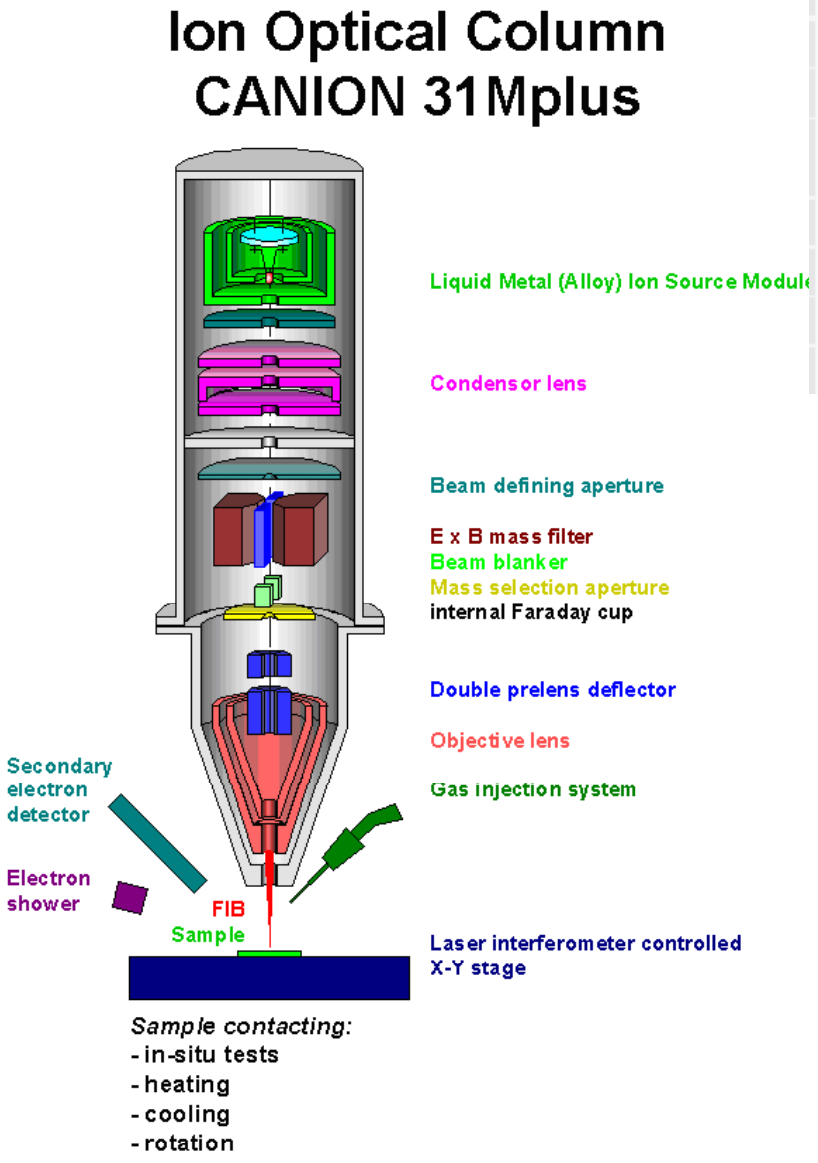

Complex and cubersome setups

Focused Ion Beam Laboratory

FIB-System IMSA - Orsay Physics

The FIB system IMSA-100 was developed in 1988, in order to obtain extra high current densities of more than 10 A/cm^2 for different ion species. The ion optical column contained a liquid Ga metal or a metal alloy ion source (LMIS/LMAIS), two electrostatic lenses, a double octopole deflector, an ExB mass filter, a blanker, two stigmators and a secondary electron/ion detection system for imaging.

After a 12-year successful operation the equipment was modernised, because of the insufficient beam resolution of about 200 nm. The IMSA-100 column including the control unit was replaced by a CANION Z31Mplus column from Orsay Physics, whereas a lot of features of the old FIB tool can be further used. The new ion column is also equipped with an ExB mass separator to apply LMAISs.

Energy	10-30 keV (singly charged)
Ion species	Ga, Co, Nd, Ge, Au, Si, Er, Ni, Fe, Cr, B, In ...
Ion current	0.001 - 22 nA
Spot size	min 14 nm (Ga)
Current density	>20 A/cm^2
Mass resolution	35
Options	▪ Special sample holders ▪ Heating targets up to 500°C (2") and up to 700°C 1/2") ▪ Cooling down to 240 K (Peltier-element) ▪ in-situ electrical contacting, 5 pins ▪ Sample tilting (1 cm^2) 360 °; increment: 0 28° ▪ FIB assisted etching (XeF_2) ▪ FIB assisted metal deposition (W; Au) ▪ Charge neutralisation by low energy electron shower
Sample stage	Laser interferometer controlled x-y stage 160 x 160 mm^2 Reproducibility: < 50 nm
Scan field	max. 500 x 500 µm^2 (energy dependent) for larger structures: stitching

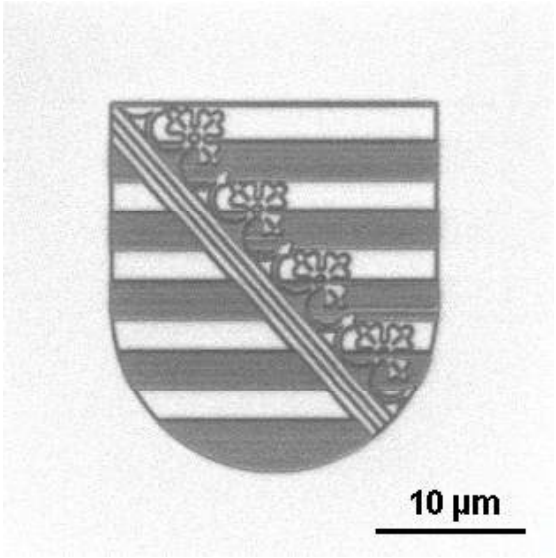

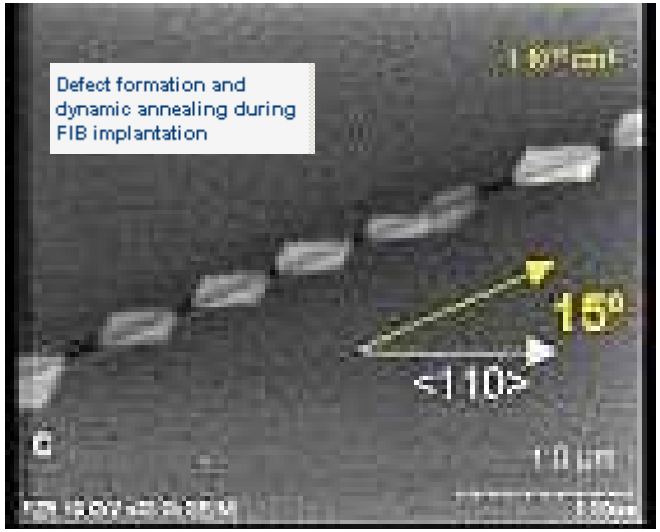

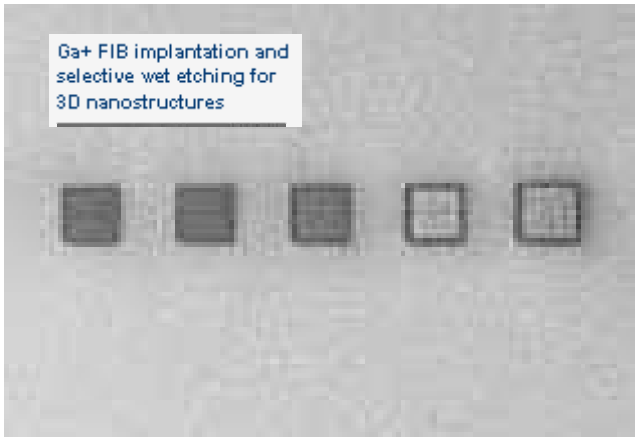

Resolution below 10 nm
Patterns with arbitrary shapes

Pros and cons of FIB

- Like EBL, FIB is used as direct writing exposure
- It is in its early development stage

FIBL and EBL Comparison

Potential:

- Less prone to backscattering (larger mass than electron)
- Resist for FIB lithography is more sensitive
- Energy higher than electrons
- ➡ Better resolution and faster exposure speed than E-beam

Issues:

- Lack of reliable ion sources
- Harder to be focused
- Shorter penetrate (absorption) depth in resist (~ 30 – 500 nm) – multilayer resist process
- Unexpected ion implantation on substrate beneath resist

4. Alternative approaches based on atom optics

Basic idea: use of a **neutral** particle beam

--> sub-nm (λ_{dB}) diffraction *without the problems of electron optics*

Further potential advantages:

- use of “optical masks” (non obtrusive, species-selective, defect-free…)
- possibility of direct deposition (bottoms-up at the atom level) or resist-assisted
- parallel character like in optical lithography

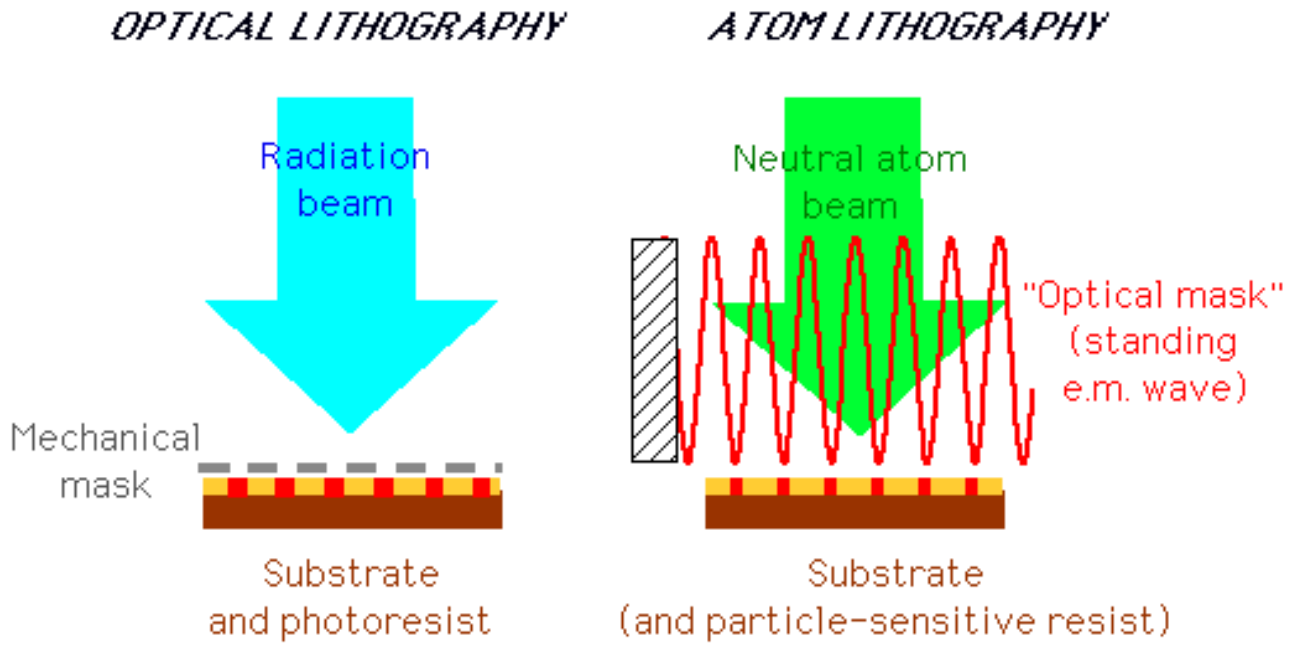

Main ingredient:
Atom optics, i.e., laser manipulation (cooling) of neutral atoms

A few words on atom optics

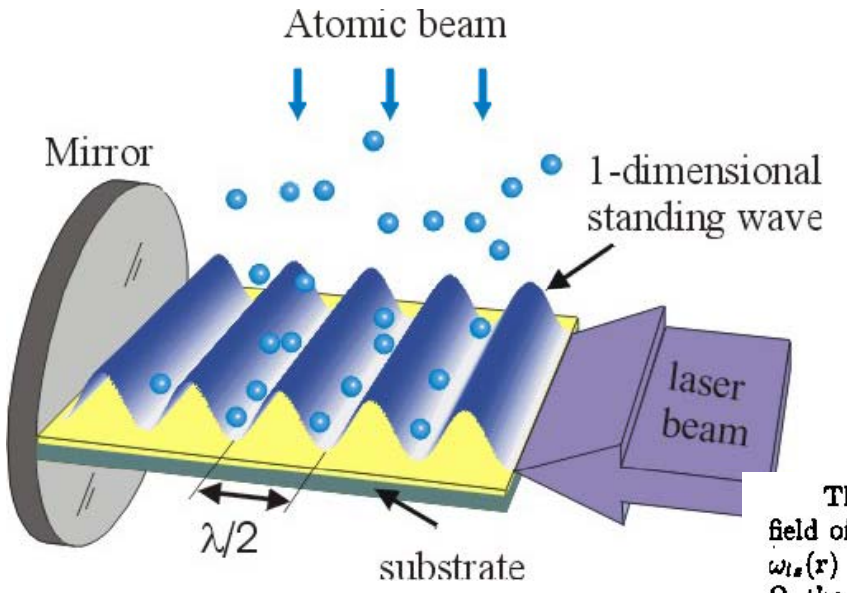

Optical mask (standing e.m. wave)
→ dipolar forces (conservative)
along a direction transverse to atom beam

Meschede Metcalf
JPD (2003)

The optical dipole force acting on an atom with resonance frequency ω_A in a laser field of detuning $\delta = \omega_L - \omega_A$ is derived from the spatial variation of the light shift $\omega_{ls}(r)$ [1]. For a single laser beam travelling in the x-direction with Rabi frequency Ω, the light shift is given by

$$\omega_{ls} = \left[\sqrt{\Omega^2 + \delta^2} - \delta\right]/2\,. \qquad (1)$$

For sufficiently large detuning $\delta \gg \Omega$, approximation of Eq. 1 leads to $\omega_{ls} \approx \Omega^2/4\delta = \gamma^2 s/8\delta$, where $s \equiv I/I_{sat}$, I is the laser beam intensity, $I_{sat} \equiv \pi hc/3\lambda^3\tau$ is the saturation intensity, and $\tau \equiv 1/\gamma$ is the atomic excited state lifetime.

In a standing wave with $\delta \gg \Omega$, $\omega_{ls} = \omega_{ls}(x)$ varies sinusoidally from node to antinode and also spontaneous emission is inhibited so that $\hbar\omega_{ls}(x)$ may be treated as a potential $U(x)$. The resulting dipole force is

$$\mathbf{F}(x) = -\nabla U(x) = -\frac{\hbar\gamma^2}{8\delta I_{sat}}\nabla I(x) \equiv U_{max}\nabla f(x), \qquad (2)$$

where $I(x) = I_{max} f(x)$ is the total intensity distribution of the standing wave light field of period $\lambda/2$, I_{max} is the maximum intensity, and $f(x)$ describes the normalized modulation of the light field. For such a standing wave, the optical electric field (and the Rabi frequency) at the antinodes is double that of each travelling wave that composes it, and so the total intensity I_{max} at the antinodes is four times that of the

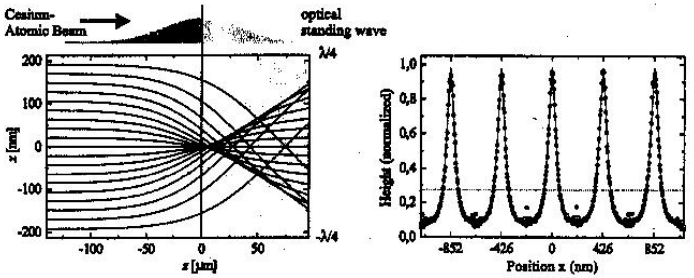

Figure 3. *Left: Numerically calculated trajectories of a laser cooled beam of atoms focussed to the center of a Gaussian envelope standing wave light field (thick lens limit). The focussed laser beam forming the optical standing wave is clipped by the substrate. Note the different scales in x- and z-directions. Right: Analysis [25] of flux concentration for a realisitic beam of thermal cesium atoms with 0.1 m/s transversal rms velocity at the focal plane z=0. The dotted line shows the flux distribution without the standing optical wave.*

The standing wave behaves like an array of microlenses for the atoms (in terms of atom optics)

Atom trajectories

Figura 3.5: Ilustrazione dei vari regimi di focalizzazione a cui possono essere sottoposti gli atomi interagenti con un'onda stazionaria: (a) regime di lente sottile, (b) lente spessa e (c) *channelling*. Le ascisse sono in unità di lunghezza d'onda, mentre le ordinate in unità di waist del fascio laser gaussiano. I colori sullo sfondo riflettono la ditribuzione di intensità del fascio laser (il massimo è rosso).

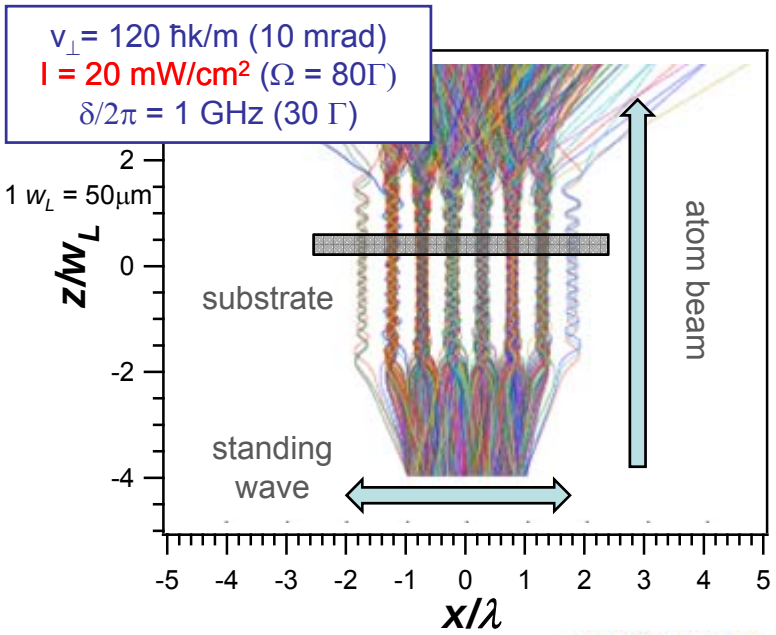

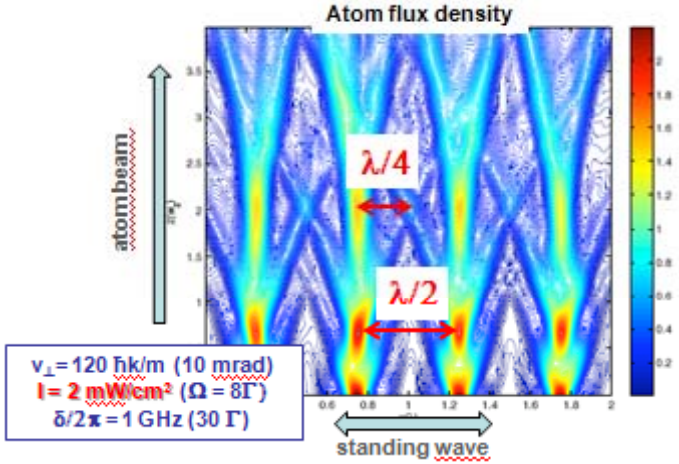

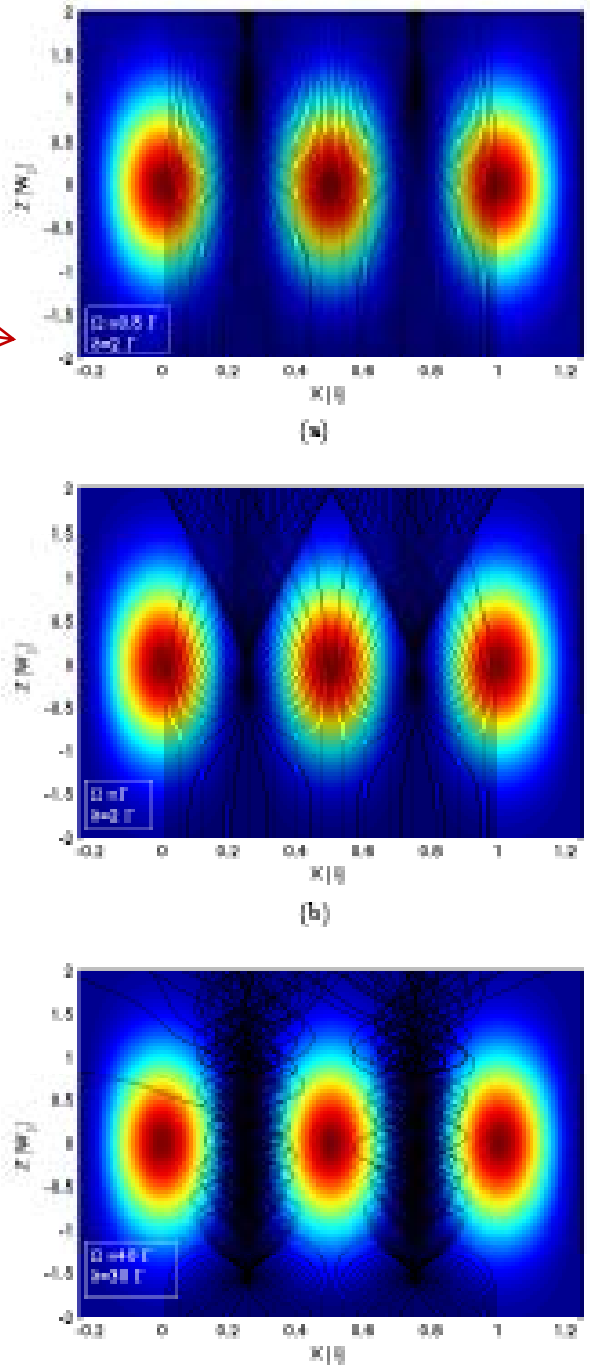

N.Porfido, Tesi di Laurea (2008)

Beams for atom lithography

1. Intensity --> reasonable exposure times

2. Collimation --> reduce aberration effects

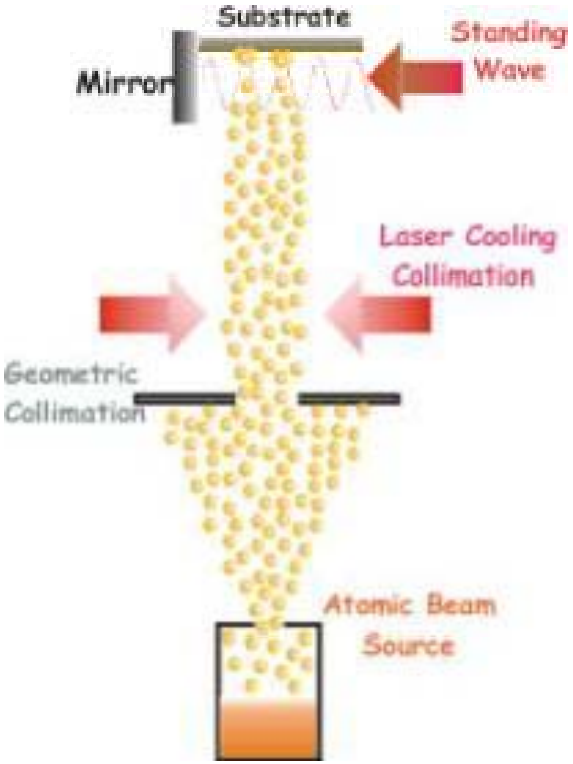

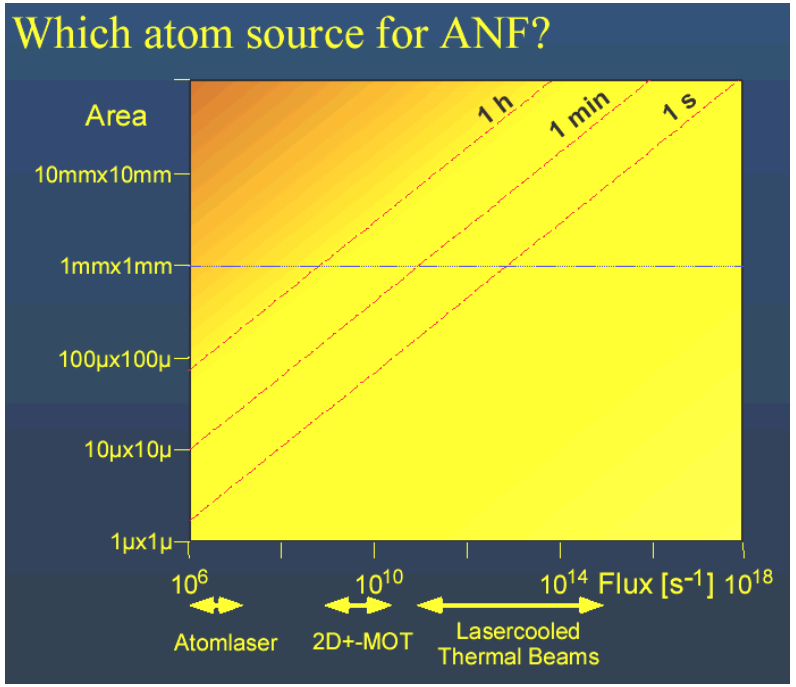

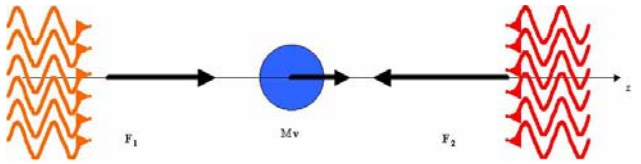

Optical molasses

$$F = F_1 - F_2 \approx 4v(\omega - \omega_{12})\hbar k^2 \langle n_{sp} \rangle \frac{1}{(\Gamma_s/2)^2 + (\omega - \omega_{12})^2} \equiv -M\gamma v$$

Laser cooling technologies enable a suitable beam conditioning

Applicability of atom lithography

Atom species must be laser manipulated (wavelength, *closed transitions*,…)

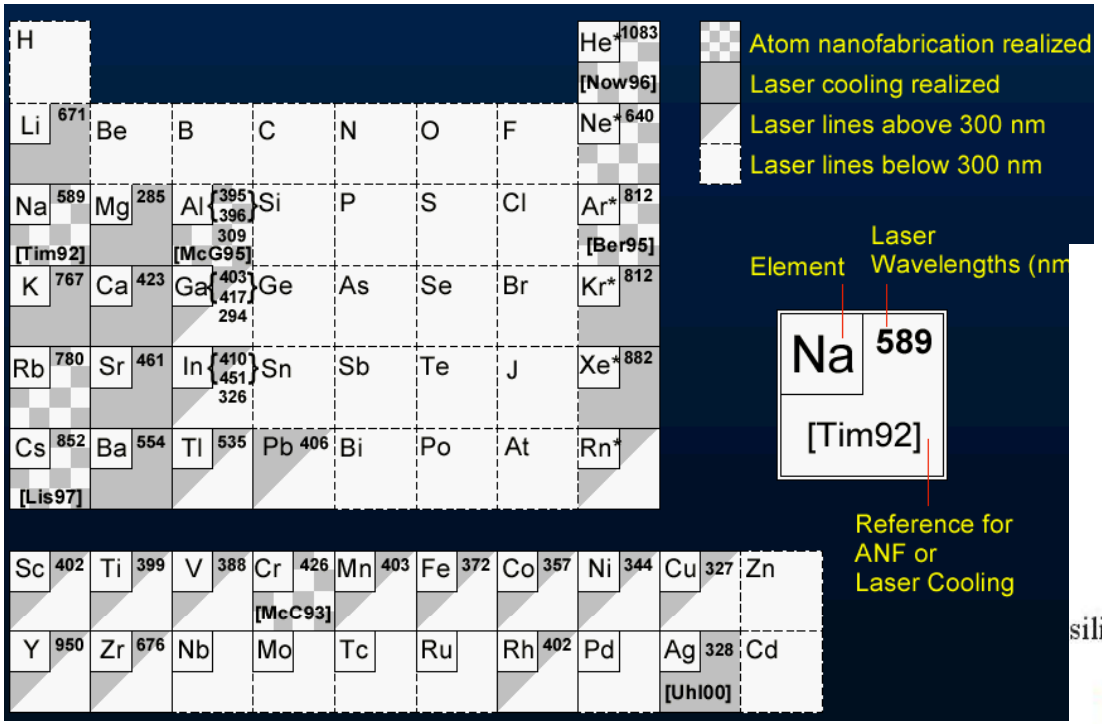

Atom	T_S K	λ nm	γ 10^7/s	v_c m/s	θ_c mrad	$5/\omega_r$ μs	$2r_c$ mm	P_c mW	Θ_D mrad	Θ_R mrad	P_{ANF} mW
$^4He^*$	300	1083	1.0	1.7	1.5	19	0.03	0.03	0.36	0.11	0.40
^{23}Na	630	589	6.2	5.8	13	32	0.18	1.0	0.89	0.09	0.12
^{27}Al	1640	309	8.2	4.0	4.0	10	0.04	6	0.44	0.07	0.95
$^{40}Ar^*$	300	812	3.6	4.8	17	105	0.49	0.5	0.68	0.05	0.15
^{52}Cr	1825	426	3.1	2.1	3.5	37	0.08	2.4	0.26	0.03	2.0
^{56}Fe	1920	372	1.6	1.0	1.3	31	0.03	1.5	0.18	0.04	4.6
^{70}Ga	1555	403	4.9	3.1	5.2	45	0.14	4.3	0.35	0.03	1.1
		417	9.2	6.1	10	48	0.29	7.8	0.48	0.03	0.59
^{108}Ag	1435	328	1.4	7.2	15	46	0.33	18	0.61	0.03	0.46
^{115}In	1355	410	5.8	3.8	8.5	77	0.29	6.0	0.40	0.03	0.83
		451	10.2	7.3	16	93	0.68	9.5	0.54	0.02	0.43
^{133}Cs	410	852	3.3	4.5	20	383	1.7	3.3	0.55	0.02	0.21
^{197}Au	1800	268	16.7	7.1	19	57	0.40	32	0.59	0.04	0.60

Materials to be employed in resist-assisted atom lithography alkanethiols self-assembling monolayers (SAM) – *we will discuss more on them later!*

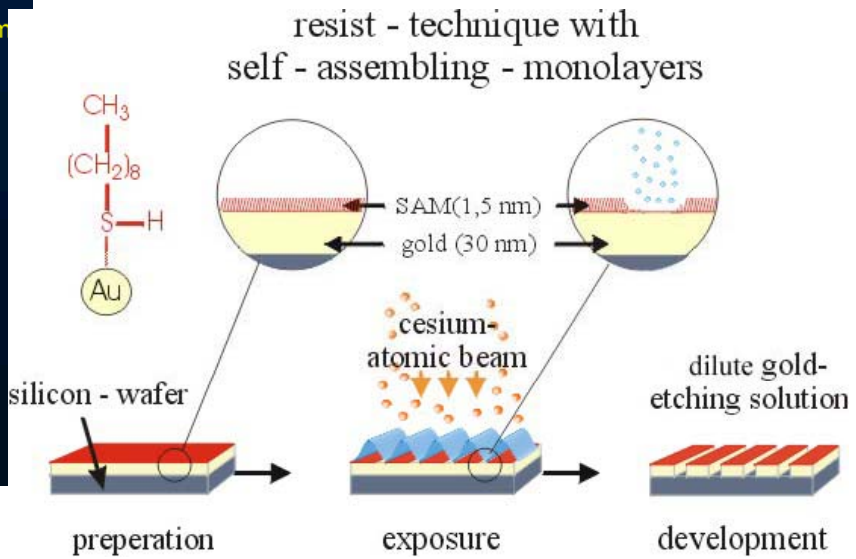

The technique can be applied only to a few atom species (at least, so far)

Gallery of examples

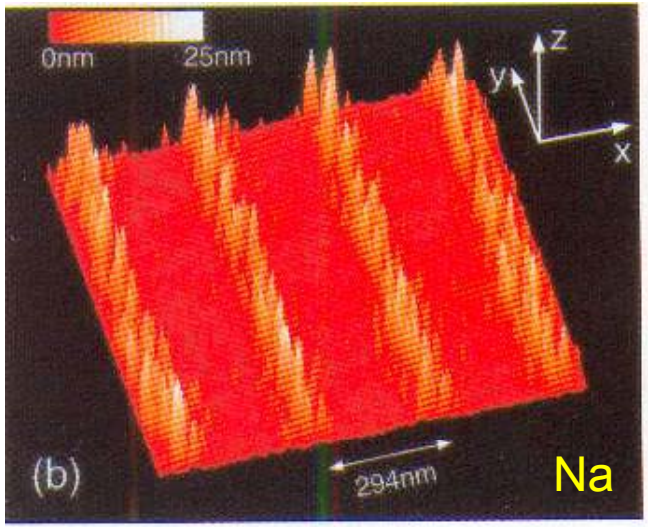

Timp et al. PRL 69 1636 (1992)

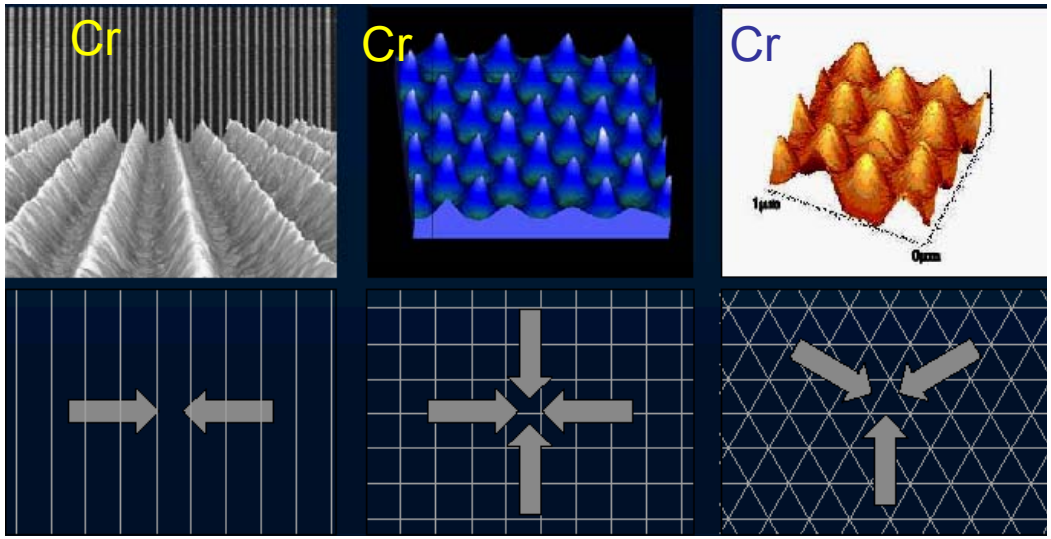

1D standing wave
McClelland et al.
Science 87 262 (1993)

2D standing waves
Gupta et al.
APL 67 1378 (1995)
Drodofsky et al.
Appl Phys B 65 755 (1997)

Holographic lithography

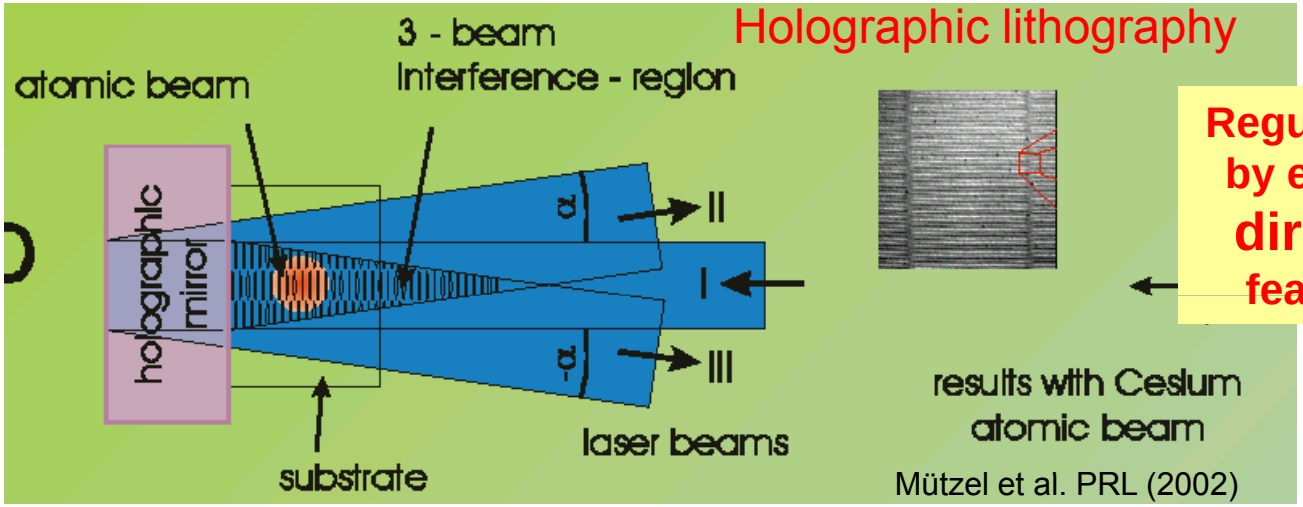

results with Ceslum
atomic beam

Mützel et al. PRL (2002)

Regular nanostructures built by either resist-assisted or direct deposition with feature size below 20 nm

Our “own” results (resist-assisted)

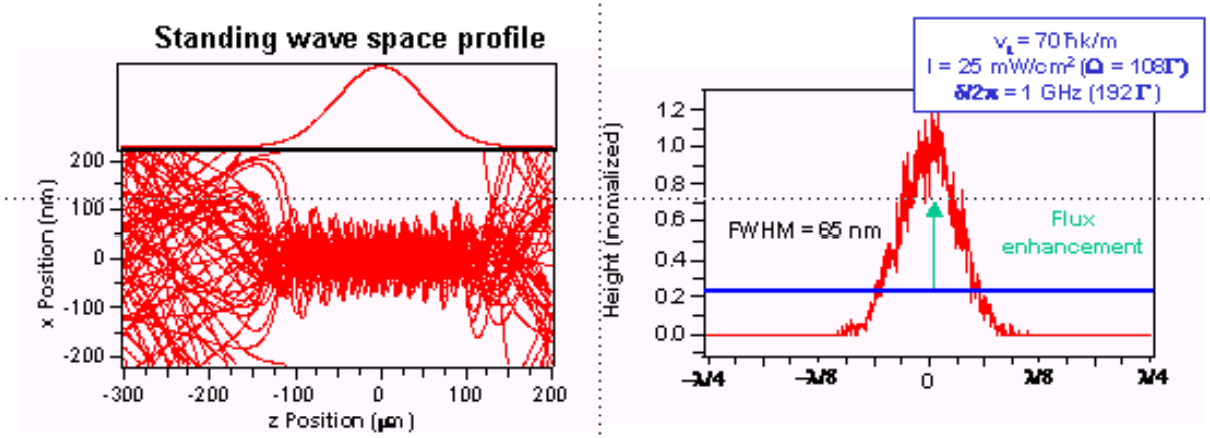

Due to the use of a “laser-cooled” atom beam (speed ~ 10 m/s), atoms are expected to be “channeled” instead of focused by the standing wave

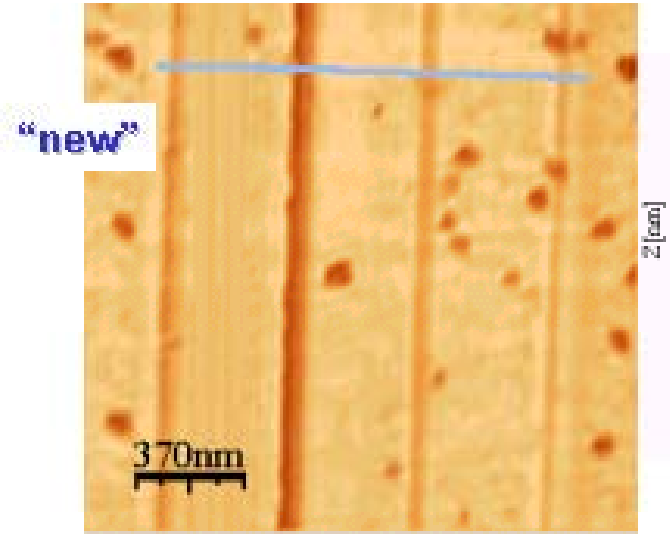

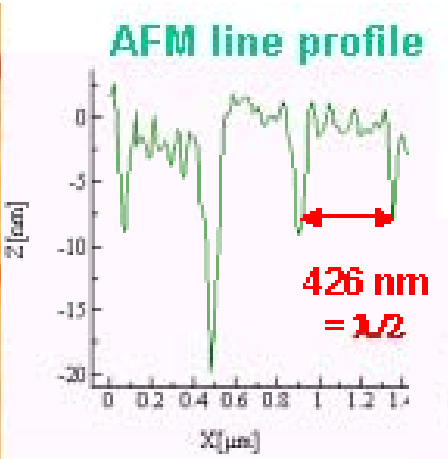

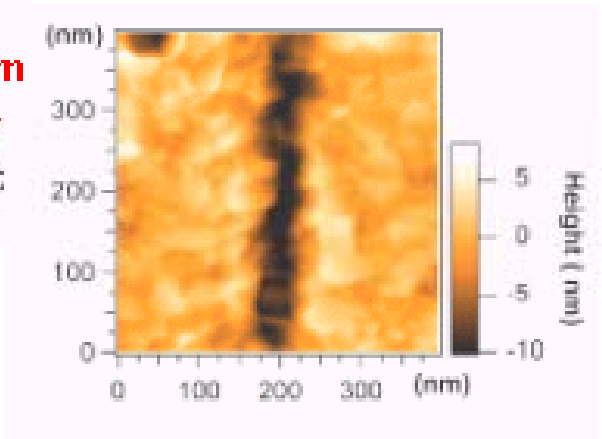

AFM image – plan view
Sputtered gold 30 nm thick
2h deposition and 13 min etching
Estimated dose: 2 atoms/SAM molecule

Our “own” results (direct-deposition, low coverage)

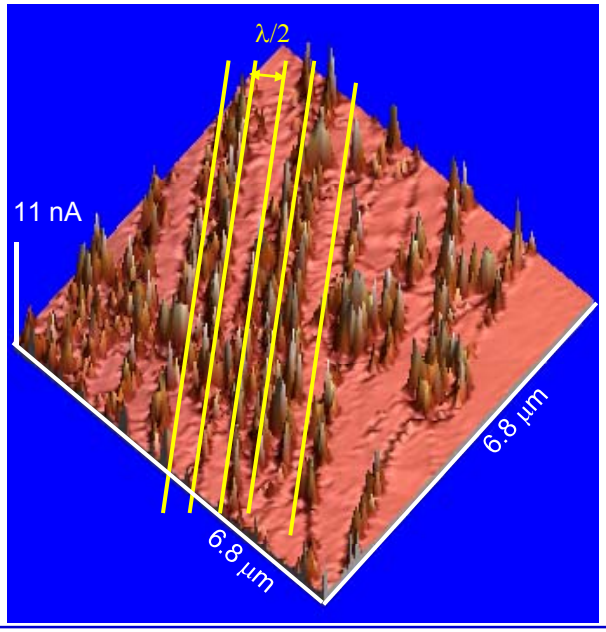

UHV-STM 3D current map
HOPG substrate (peeled off)
1.5h deposition – detuning 3 GHz
estimated local surface coverage θ ~0.15
Standing wave intensity 15 mW/cm^2

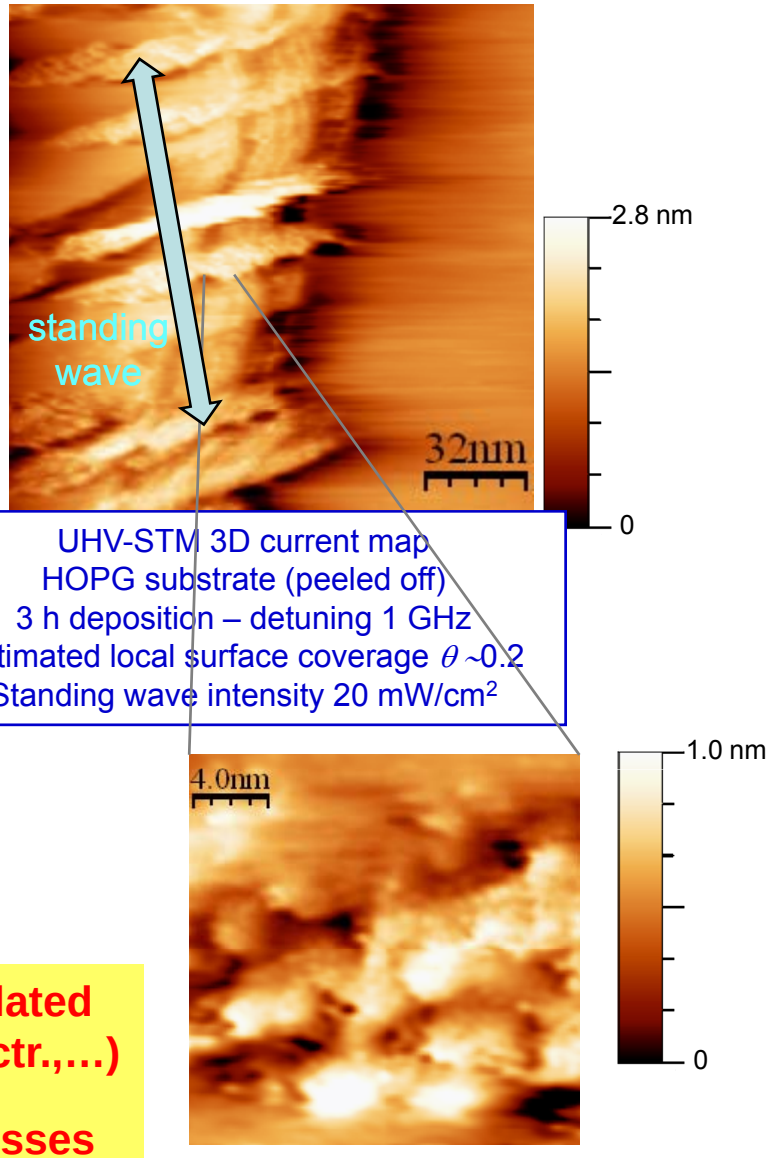

UHV-STM 3D current map
HOPG substrate (peeled off)
3 h deposition – detuning 1 GHz
estimated local surface coverage θ ~0.2
Standing wave intensity 20 mW/cm^2

Low substrate coverage regime interesting for isolated nanostructures (e.g., precise doping, molecular electr.,…)

Feasible, but substrate features and surface processes start playing a dominant role

5i. An emerging simple nanotechnology: nanoimprint

9 Nanoimprint Lithography

There are several approaches for patterning structures without lithographic methods, e.g. a silicon surface can be modified by depassivation by the tunneling current in a UHV-STM (Ultra High Vacuum Scanning Tunneling Microscope [20], [21], or the surface can be modified by the movement of an Atomic Force Microscope (AFM)-tip . A certain interest has been focused on the nanoimprint lithography (NIL), which is described in more detail in this section.

With the NIL, a mold is processed by conventional technology, i.e. e-beam lithography and etching techniques, and is pressed onto a resist coated substrate. The structures in the mold are transferred into the resist and can be utilized after removing the mold. There are two different kinds of NIL, the hot embossing technique and a UV-based technique. A sketch of both techniques is given in Figure 29.

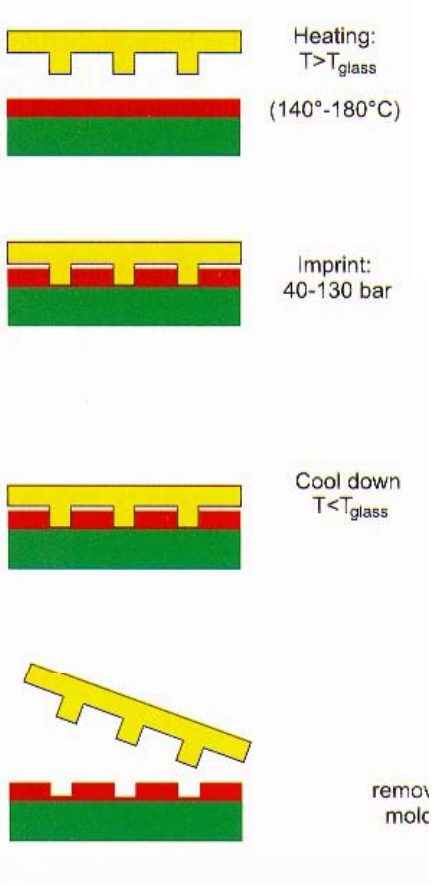

Hot Embossing Technique

Here the sample is heated above the glass transition temperature of the resist, which is a thermoplastic polymer. Above that temperature the polymer behaves as a vicous liquid and can flow under pressure. The mold itself can be made of different materials, usually a silicon wafer with a thick SiO_2 layer is used. This SiO_2 layer is patterned and structured by e-beam lithography and anisotropic reactive ion etching. The aspect ratio of the features are 3:1 to 6:1, and the mold size is several cm^2. As thermoplastic polymers either PMMA (a well known e-beam resist) or novolak resin-based resists are in use. PMMA has a small thermal expansion coefficient of $\sim 5 \times 10^{-5}\ K^{-1}$ and a small pressure shrinkage coefficient of $\sim 3.8 \times 10^{-7}\ psi^{-1}$. To ensure a proper removal of the mold, the resist is modified by release agents, which decrease the adhesion between mold and resist. Resist layers between 50 and 250 nm thickness are used. The imprint temperature and pressure are dependent on the resist. For PMMA the glass transition temperature is about 105°C, so the temperature at which the sample and the mold are heated is between 140 and 180°C. Then the mold is pressed onto the sample with pressures of about 40 – 130 bar. The temperature is then lowered below the glass transition temperature and the mold is removed. The features of the mold are now imprinted in the resist. The residual resist layer in these features is removed by anisotropic reactive ion etching. Afterwards, the structures can be transferred to the substrate either by direct etching or by metal deposition and lift-off. Structures down to a feature size of 10 nm for holes and 45 nm for mesas are imprinted with a high accuracy [22]–[24].

Thermoplastics

The range of potential materials available for hot-embossing techniques is very wide. Much of the development of thermal NIL methods has been done with poly(methyl methacrylate) (PMMA) as the molded material.[1,7,9,14,20] PMMA is a readily available, relatively cheap, and well-studied polymer system with an easily accessible glass-transition temperature (T_g) of 110°C. Molding temperatures are typically 20–50°C above T_g. Other simple polymers such as polystyrene,[7,9,21] polycarbonate,[21] and poly(vinyl alcohol)[22] have also been used in hot-embossing processes.

Non-Thermoplastic Materials

Another option available for thermal NIL processing is thermosetting polymers. "Thermosets" begin to cross-link or cure upon heating above some characteristic temperature, which complicates the choice of imprint conditions, as the initial molding temperature should be below the curing temperature but still hot enough to allow sufficient thermoplastic flow to fill the mold. Thermosets have the processing advantage of not necessarily requiring a cool-down step prior to mold release, potentially speeding processing. Many thermoset systems also have very good mechanical and thermal properties once fully cured. Some thermosetting polymers used in nanoimprint have been reported as poly-benzene-dicarboxylic-diallylesters.[32]

Other interesting materials molded with NIL methods include hydroger silsesquioxane (HSQ) and spin-on-glass (tetraethoxysilane) compounds.[33] In this case, the materials were able to be printed at room temperature using relatively low pressures (100–500 kPa) due to the presence of a solvent in the material. Patterned HSQ and spin-on-glass materials have potential applications as optical components. Also reportedly molded in a room temperature NIL process were several commercially available low-molar-mass thiophene derivates.[34] These thiophene based compounds are organic semicon

UV-assisted nanoimprint

UV-based NIL

Heating and cooling of mold and sample is time-consuming. Therefore to achieve a somehow higher throughput, curing of the resist by UV irradiation is used. The thermoplastic resist is replaced by UV-curable monomers. The mold has to be fabricated of a UV-transparent material, e.g. quartz. The features are transferred to the mold by e-beam lithography and a Ti/PMMA resist stack. The patterned PMMA is used to transfer the features into the Ti, and the Ti is used to structure the quartz mold. The resists are acrylate- or epoxide-material systems, which can be modified with respect to low viscosity, UV curability, adhesion to the substrate and detachment from the mold. The low viscosity is essential for using low imprint pressures of 40 mbar – 1 bar. After pressing the mold on the sample, the sample is irradiated by UV-radiation through the mold and a baking, and hence a polymerization of the resist is initiated. This step lasts only about 90 seconds. After detaching the mold, the residual resist is removed by RIE and the further pattern transfer can be done. Again mold areas of several square centimeters can be imprinted in one run, and one imprint step takes about 10 minutes. The minimum feature size reported in the literature is 80 nm for dots. [25].

NIL offers the opportunity to define decananometer features in a rather *simple* manner, at least in comparison to the advanced lithography methods described above. The field size of ~2×2 cm^2 is comparable to a die which is illuminated by a stepper. On the other hand, this method is time-consuming (>10 min for one imprint) and up to now only structures on a plain surface have been investigated, while advanced lithography is able to define structures on textured substrates. Nevertheless, because of its technological simplicity, the NIL will be an alternative for research and small series production.

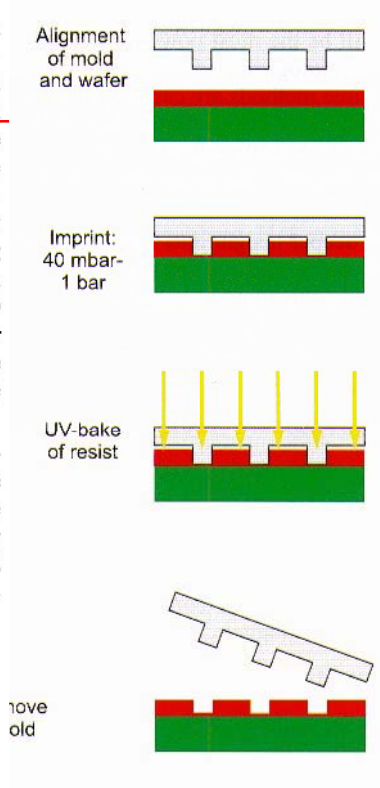

Photosetting Materials

Using already formed polymers allows for a great variety of potential imprint materials from which to choose, but as already mentioned, there are several problems related to the molding of high-viscosity materials. Because of these problems, more attention has been focused lately on the development of UV-NIL. While UV-NIL definitely has advantages, it makes for a more complex materials challenge. In addition to the requirement of low viscosity in the precursor material, the precursor must be photosensitive or sensitizable with additives. The low-viscosity requirement rules out high-molecular-weight polymers, and the photosensitive requirement rules out materials that strongly absorb at the intended actinic wavelength (the wavelength of activity/sensitivity). The final cured material must adhere to the substrate while not adhering to the mold. This challenge is usually solved by treating the surface of the mold and/or substrate as required, but the suitability of potential surface treatments must be evaluated for each proposed precursor formulation. Also to be considered are photocuring rates and the possibility of cure-induced shrinkage. The first UV-NIL processes used free-radical curing of acrylate monomers,[35] and much of the early work with UV-NIL has been with variants of acrylate chemistry, with new classes of materials only more recently being pursued.

Termomechanical or UV-assisted methods can be employed to replicate a master pattern with nanosized features

Examples of nanoimprinting I

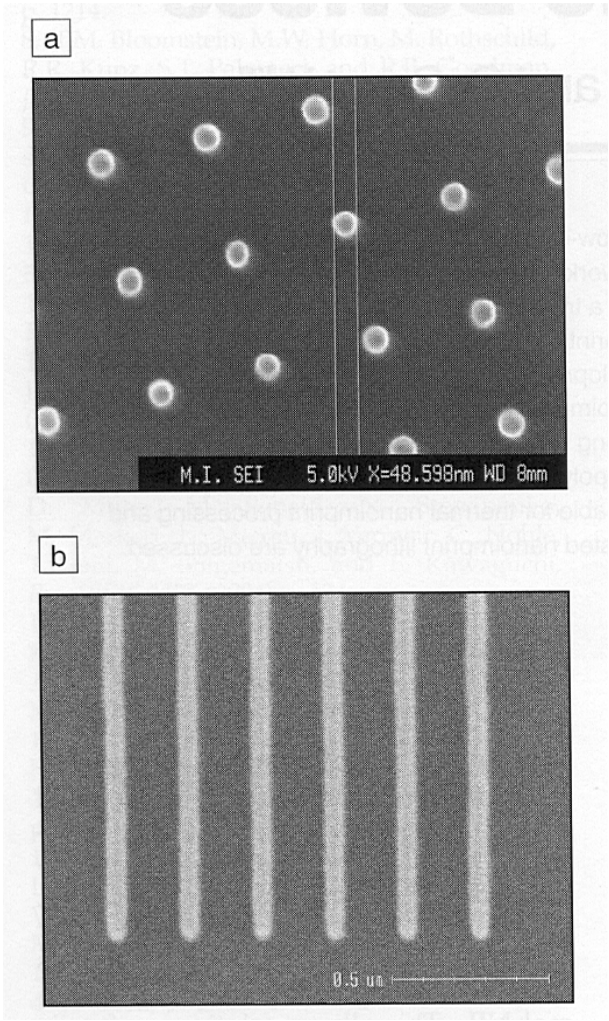

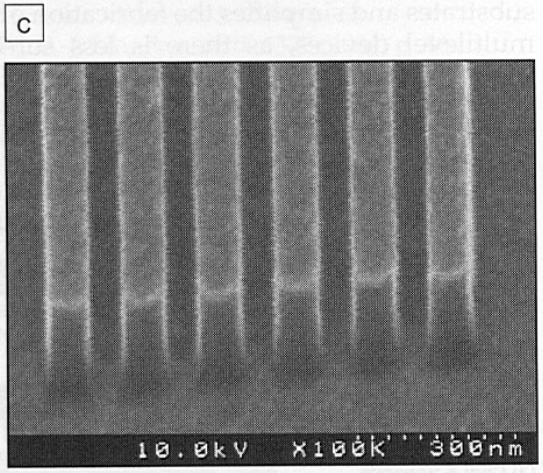

Figure 2. Scanning electron microscopy images of patterning results from a UV-NIL process (step and flash imprint lithography variant). (a) 50-nm-diameter raised pillars/posts; fine lines flanking one post are measurement bars from the SEM screen. (b) 30-nm lines on semi-isolated pitch. (c) 100-nm lines on 150-nm pitch. All features are still in the molded resist.

May nanomprint be an alternative to conventional lithography?

Examples of nanoimprinting II

NANO LETTERS
2006
Vol. 6, No. 3
351−354

Circuit Fabrication at 17 nm Half-Pitch by Nanoimprint Lithography

Gun-Young Jung,[†,‡] Ezekiel Johnston-Halperin,[§] Wei Wu,[†] Zhaoning Yu,[†] Shih-Yuan Wang,[†] William M. Tong,[†,||] Zhiyong Li,[†] Jonathan E. Green,[§] Bonnie A. Sheriff,[§] Akram Boukai,[§] Yuri Bunimovich,[§] James R. Heath,[§] and R. Stanley Williams*[,†]

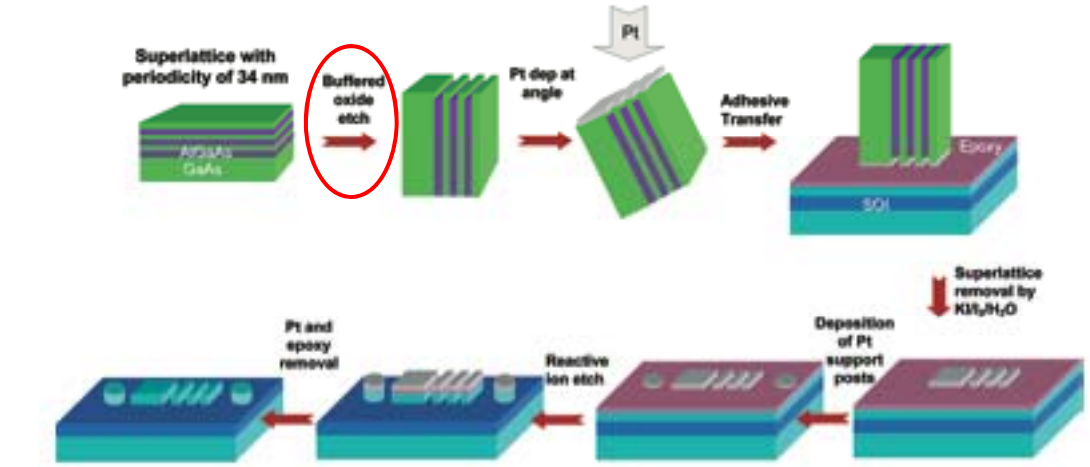

SNAP process procedure for transferring nanoscale features from a cleaved superlattice to a flat substrate.

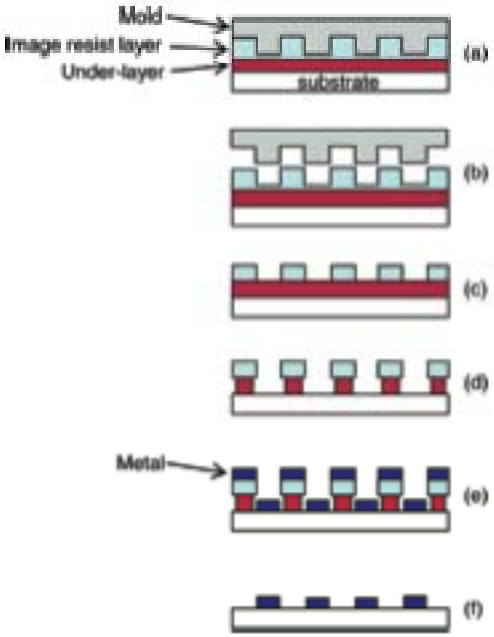

Figure 2. Schematic diagram of process flow: (a) application of mold to resist; (b) mold separation from the imprinted resist; (c) residual layer etching; (d) pattern transfer to the underlayer; (e) metal deposition; (f) metal lift-off.

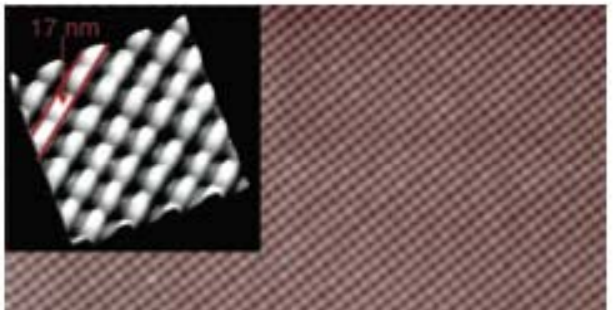

Figure 4. A scanning electron micrograph of the central region of a 13 000 junction metal cross-bar structure. This circuit was generated by carrying out two consecutive nanoimprinting processes. The same mold was employed for both. The inset shows an AFM image of a magnified region of the cross bar.

…maybe, but mask preparation is quite cumbersome!

5ii. Direct laser writing and 3D holographic lithography

Holographic lithography and multiphoton effects can be combined to get direct access to 3D structure fabrication

- La focalizzazione del fascio genera emissione nel range UV- visibile da parte del mezzo in seguito all'assorbimento di due fotoni. Tale radiazione stimola la polimerizzazione della zona esposta tramite la formazione di radicali.

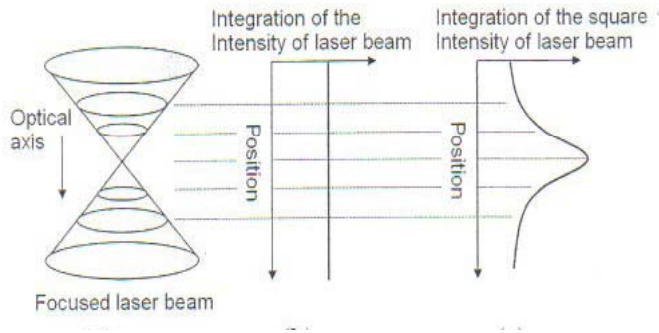

initiation : $S \xrightarrow{h\nu, h\nu} S^* \cdots \xrightarrow{I} I^* \rightarrow R^{\cdot}$ (1)

propagation : $R^{\cdot} + M \rightarrow RM^{\cdot} \xrightarrow{M} RMM \cdots \rightarrow RM_n^{\cdot}$ (2)

termination : $RM_n^{\cdot} + RM_m^{\cdot} \rightarrow RM_{n+m}R$ (3)

which describe the interactions of the photosensitizer (S), photoinitiator (I), radical ($R^{\cdot}$), and the monomer (M). S* and I* are the excited states of the photosensitizer and photoinitiator after absorbing the photon energy, respectively.

La probabilità di assorbimento a due fotoni risulta proporzionale al quadrato dell'intensità della luce pertanto questo processo può essere attivato solo in un ristretto volume ("voxel", volumetric pixel) attorno al fuoco.

Si ottiene così una alta risoluzione spaziale al di sotto del limite diffrattivo (sono state ottenute strutture dalle dimensioni laterali di 120 nm lavorando con lunghezza d'onda di 780 nm).

K.-S. Lee et al. Polym. Adv. Technol. ***17****,72-82 (2006)*

Materiale tratto dal seminario di Christian Martella, 2006

Examples of 3D (nano)structures

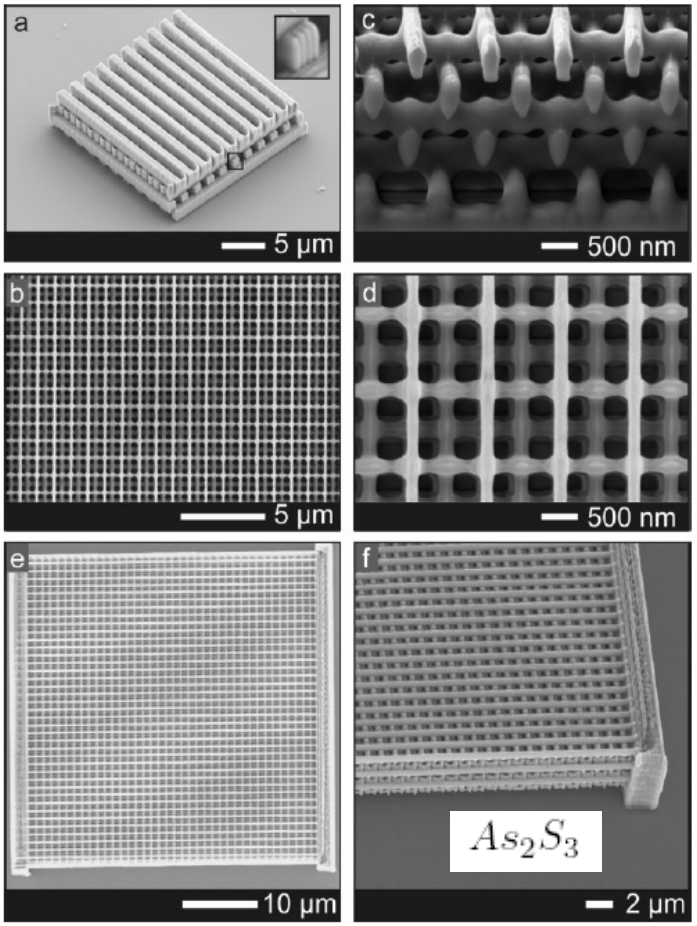

Direct writing of inorganics performed during the growth process (CVD-like)

Use of two-photon chromophores for organics

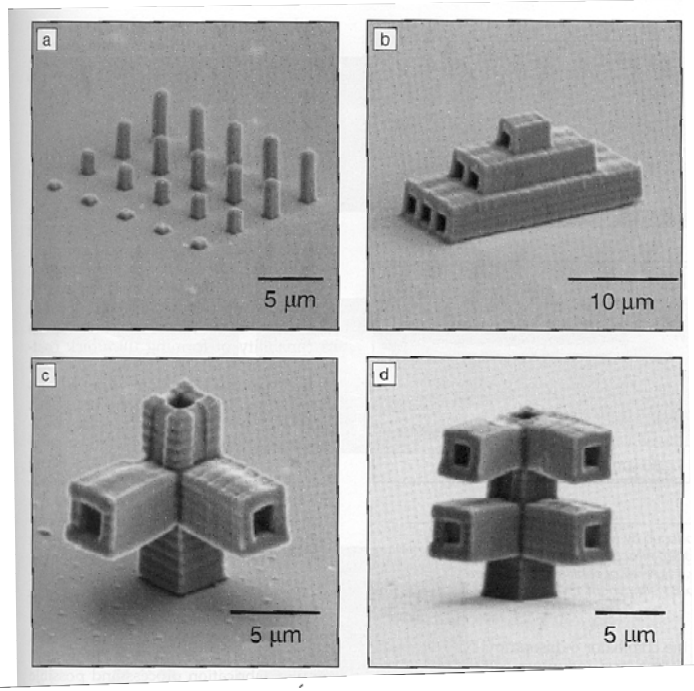

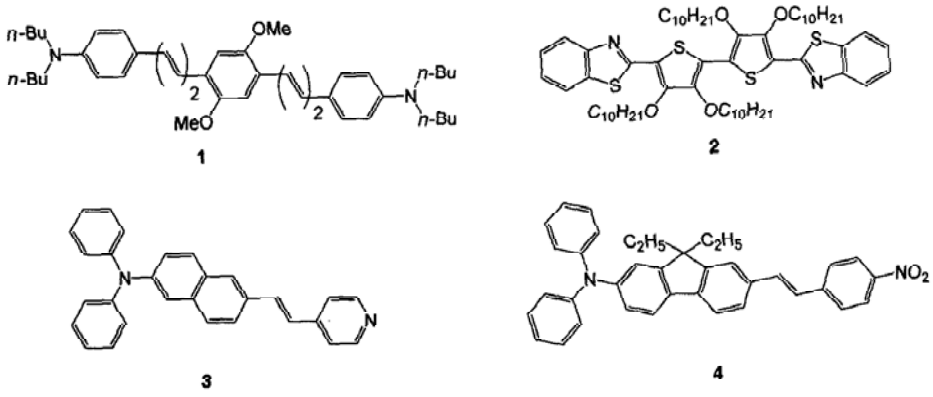

Scheme I. Structures of two-photon chromophores. (1) D-π-A-π-D–type chromophore (λ_{max} = 448 nm, δ = 1250 × 10^{-50} cm^4 s $photon^{-1}$); (2) A-π-A–type chromophore (λ_{max} = 430 nm, δ = 2850 × 10^{-50} cm^4 s $photon^{-1}$); (3) D-π-A–type chromophore (λ_{max} = 388 nm, δ = 6840 × 10^{-50} cm^4 s $photon^{-1}$); (4) fluorene-based chromophore (λ_{max} = 414 nm, δ = 1300 × 10^{-50} cm^4 s $photon^{-1}$). D = donor; A = acceptor, λ_{max} = wavelength of maximum absorbance, and δ = absorption cross section.

5iii. Towards ease of use: inkjet lithography

Polymer-Relief Microstructures by Inkjet Etching**

By *Berend-Jan de Gans, Stephanie Hoeppener,* and *Ulrich S. Schubert**

Adv. Mater. 2006, 18, 910–914

Inkjet printing is developing at a rapid pace. The last decade saw continuous improvements in quality and resolution, and the technology has now arrived at the point where it challenges conventional silver halide photography. But inkjet technology is not only a printing technology. A lot of effort is being put into turning inkjet printing into a versatile tool for various industrial processes for accurately depositing minute quantities of materials in defined spots on surfaces, in particular in plastic electronics and polymer light-emitting diodes.[1–5] Inkjet printing may also become a cost-saving alternative to photolithography for the production of next-generation active-matrix liquid-crystal displays.[6] Of particular interest is the use of inkjet printing in the fields of biotechnology and combinatorial chemistry as a tool for the preparation of ink-jet-printed polymer microarrays or libraries,[7] i.e., arrays of individually addressable dots or rectangles with well-known compositions on substrates.

Rather than depositing a functional component, an inkjet-printed solvent droplet can also be used to site-selectively remove material that was deposited previously by a different technique.[8,9] Via holes were etched in an insulating layer of poly(vinyl phenol) (PVP) by inkjet printing droplets of ethanol, which is known to be a good solvent for PVP. The ethanol locally dissolves the PVP. As a result, a craterlike hole is formed by redeposition of the dissolved polymer at the contact line. The mechanism behind the formation process of the hole is commonly known as the coffee-ring effect. It refers to the formation of a ringlike deposit of solute from a drying droplet by assuming a maximum in the evaporation rate at the outside of the droplet and pinning of the three-phase contact line.[10–12] The potential of this "inkjet-etching" technique is evident for any area of technology that uses polymer-relief

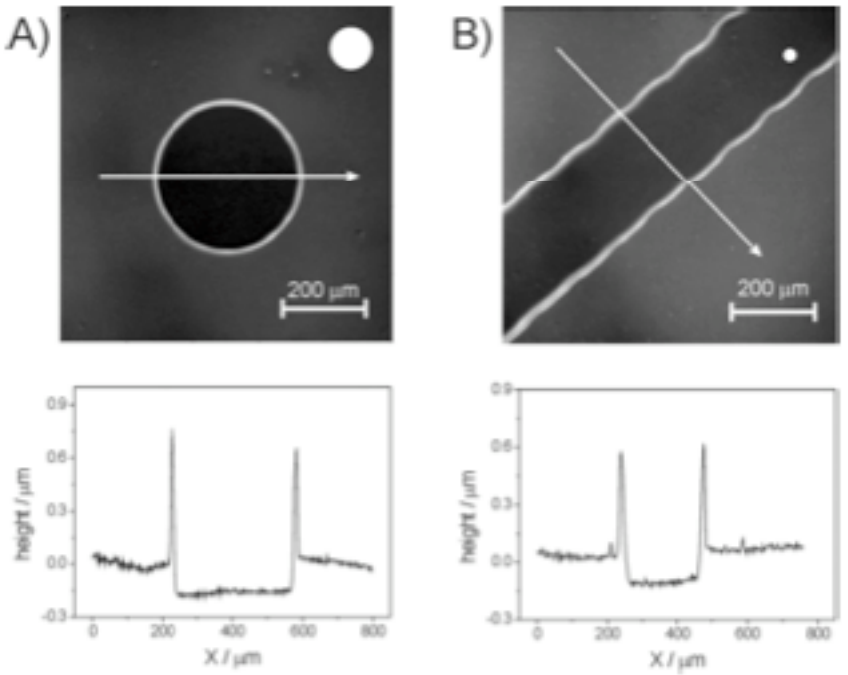

Figure 1. A) Confocal scanning microscopy image of a hole etched into a polystyrene film by a 100 µm droplet of isopropyl acetate (shown to scale as the white circle in the upper right). B) Groove etched in poly(benzyl methacrylate) layer by a line of 30 µm *n*-butyl acetate droplets (circle, upper right) with a spacing of 120 µm.

Inkjet direct printing of material (or etching, as in this case) proposed as an ultra-flexible and ultra-cheap technique:
- liquid or semiliquid materials must be used;
- slow process;
- difficult to produce nanodroplets

Conclusions

✓ Many efforts have being devoted to develop techniques able to overcome the limitations of optical lithography in terms of space resolution

✓ The use of charged particle beams offers direct access to extreme resolution (at the expenses of technological issues and limitations)

✓ Atom beams might be used as well (*in an optimistic and perspective view)*

✓ Emerging techniques are being proposed with the primary aim of ease-of-use, cheapiness, efficiency (more than high resolution)